nature methods

Article

https://doi.org/10.1038/s41592-023-02100-w

Improved green and red GRAB sensors for monitoring dopaminergic activity in vivo

Received: 24 March 2023

Accepted: 23 October 2023

Published online: 30 November 2023

Check for updates

Yizhou Zhuo[1,2,14], Bin Luo[1,2,3,14], Xinyang Yi[1,2], Hui Dong[1,2,3], Xiaolei Miao[1,2,4], Jinxia Wan[1,2,3], John T. Williams[5], Malcolm G. Campbell[6], Ruyi Cai[1,2], Tongrui Qian[1,2], Fengling Li[7], Sophia J. Weber[8], Lei Wang[1,2,9], Bozhi Li[1,2,10], Yu Wei[1,2], Guochuan Li[1,2], Huan Wang[1,2], Yu Zheng[1,2], Yulin Zhao[1,2], Marina E. Wolf[8], Yingjie Zhu[7], Mitsuko Watabe-Uchida[6] & Yulong Li[1,2,3,11,12,13]

Dopamine (DA) plays multiple roles in a wide range of physiological and pathological processes via a large network of dopaminergic projections. To dissect the spatiotemporal dynamics of DA release in both dense and sparsely innervated brain regions, we developed a series of green and red fluorescent G-protein-coupled receptor activation-based DA ($GRAB_{DA}$) sensors using a variety of DA receptor subtypes. These sensors have high sensitivity, selectivity and signal-to-noise ratio with subsecond response kinetics and the ability to detect a wide range of DA concentrations. We then used these sensors in mice to measure both optogenetically evoked and behaviorally relevant DA release while measuring neurochemical signaling in the nucleus accumbens, amygdala and cortex. Using these sensors, we also detected spatially resolved heterogeneous cortical DA release in mice performing various behaviors. These next-generation $GRAB_{DA}$ sensors provide a robust set of tools for imaging dopaminergic activity under a variety of physiological and pathological conditions.

DA is a crucial monoamine neuromodulator released by dopaminergic neurons that project throughout the central nervous system. Remarkably, there is high spatial and functional heterogeneity in dopaminergic innervation across different brain regions[1–9]. By combining G-protein-coupled receptors (GPCRs) with circularly permutated fluorescent protein, we and others developed a series of genetically encoded green and red fluorescent DA sensors called $GRAB_{DA}$ and dLight[10–13]. These early generation sensors expand our knowledge of DA transmission in reward, learning and movement[14–17], in densely innervated regions such as striatum and nucleus accumbens (NAc). However, due to limited sensitivity and resolution in DA detection, the dynamics of dopaminergic transmission in the sparsely innervated regions, such as the medial prefrontal cortex (mPFC) and amygdala, remain largely unknown. In addition, even in dense areas, better sensors

[1]State Key Laboratory of Membrane Biology, Peking University School of Life Sciences, Beijing, China. [2]PKU-IDG/McGovern Institute for Brain Research, Beijing, China. [3]Peking-Tsinghua Center for Life Sciences, New Cornerstone Science Laboratory, Academy for Advanced Interdisciplinary Studies, Beijing, China. [4]Department of Anesthesiology, Beijing Chaoyang Hospital, Capital Medical University, Beijing, China. [5]Vollum Institute, Oregon Health & Science University, Portland, OR, USA. [6]Center for Brain Science, Department of Molecular and Cellular Biology, Harvard University, Cambridge, MA, USA. [7]Shenzhen Key Laboratory of Drug Addiction, Shenzhen Neher Neural Plasticity Laboratory, the Brain Cognition and Brain Disease Institute, Shenzhen Institute of Advanced Technology, Chinese Academy of Sciences, Shenzhen, China. [8]Department of Behavioral Neuroscience, Oregon Health & Science University, Portland, OR, USA. [9]Peking University–Tsinghua University–National Institute of Biological Sciences Joint Graduate Program, Peking University, Beijing, China. [10]Department of Neurology, The First Medical Center, Chinese PLA General Hospital, Beijing, China. [11]Chinese Institute for Brain Research, Beijing, China. [12]Institute of Molecular Physiology, Shenzhen Bay Laboratory, Shenzhen, China. [13]National Biomedical Imaging Center, Peking University, Beijing, China. [14]These authors contributed equally: Yizhou Zhuo, Bin Luo. e-mail: yulongli@pku.edu.cn

with improved signal-to-noise ratio (SNR) are required for DA imaging with higher spatiotemporal precision. The ability to directly visualize and compare DA dynamics in both densely and sparsely innervated areas will therefore provide insights into spatiotemporal regulation of dopaminergic activity. Moreover, to explore how dopaminergic signaling is affected by neuronal activity and/or other neuromodulators requires multiplexed DA imaging combined with optogenetics and the simultaneous imaging of other neurochemical processes. Previous red-shifted DA sensors show relatively poor performance compared with green ones, limiting their use. To overcome these issues, we performed large-scale rational mutagenesis and cell-based screening to develop next-generation green and red fluorescent $GRAB_{DA}$ sensors with high sensitivity, high SNR and wider concentration range for DA detection across the brain.

Results

Engineering and characterization of DA sensors in cells

To develop next-generation DA sensors, we utilized various DA receptor subtypes from several species as the sensor scaffold and replaced each receptor's third intracellular loop (ICL3) with the ICL3 from existing sensors[10,12,13,18]. We identified several chimera prototypes with promising performances in the initial screening, by transplanting the ICL3 of $rGRAB_{DA}$ to *Solenopsis invicta* dopamine D2-like receptor (hereafter termed red fire ant D_2R) and the ICL3 of $GRAB_{NE}$ to bovine D_1R. We also obtained good candidates when re-engineering the ICL3 of dLight1.3b (ref. 10) and RdLight1 (ref. 12) to human D_1R (Fig. 1a and Supplementary Figs. 1 and 2). We then systematically optimized the length and composition of the linker sequences, key residues in the circularly permutated fluorescent protein affecting protein folding and/or fluorescence intensity[19–24], and sites in the GPCR affecting ligand binding and/or structural coupling[25–28], and screened a total of 5,000 variants (Supplementary Figs. 1 and 2). Using maximum brightness and the DA-induced change in fluorescence as selection criteria, our screening yielded a series of top-performing DA sensors with various DA receptor backbones, including green gDA3m (human D_1R-based) and gDA3h (bovine D_1R-based) sensors, red-shifted rDA2m and rDA2h (red fire ant D_2R-based) sensors, as well as rDA3m and rDA3h (human D_1R-based) sensors (Fig. 1b,c and Supplementary Fig. 3), with 'm' and 'h' referring to medium and high DA affinity, respectively. We also generated DA-insensitive versions through GPCR ligand-binding pocket mutations as negative controls, namely gDA3mut, rDA2mut and rDA3mut (Extended Data Fig. 1).

All six of our generated $GRAB_{DA}$ sensors effectively localized to the cell membrane when expressed in HEK293T cells. They exhibited large fluorescence increases to bath-applied 100 μM DA (Fig. 1d), while negative mutant sensors did not respond to DA (Extended Data Fig. 1). The sensors' affinities were within physiological DA levels, ranging from nanomolar to submicromolar concentrations (Fig. 1e and Supplementary Table 1). Comparing these sensors with previously reported $GRAB_{DA}$ and dLight sensors[10–13] in cultured cells, both gDA3m and gDA3h outperformed with a >2-fold increase in fluorescence (peak $\Delta F/F_0$ of ~1,000%) and a higher SNR compared with gDA2m and dLight1.3b (Fig. 1f–h and Supplementary Table 1). For red-shifted sensors, rDA2m and rDA2h had the largest dynamic range (peak $\Delta F/F_0$ of ~560% and ~240%, respectively) among D_2R-based red-shifted sensors (Fig. 1f–h and Supplementary Table 1). Finally, rDA3m and rDA3h exhibited higher brightness, fluorescence responses (peak $\Delta F/F_0$ of ~1,000%) and SNR compared with RdLight1 (Fig. 1f–h and Supplementary Table 1). Next, we examined the properties of our sensors when expressed in cultured neurons. Consistent with our results obtained using HEK293T cells, these sensors localized well to the neuronal membrane and responded strongly to DA application (Fig. 2a–d), with similar DA affinity as in HEK293T cells. In addition, we obtained the same rank order in terms of the peak response to DA measured in cultured neurons and HEK293T cells. Moreover, the next-generation $GRAB_{DA}$ sensors had higher SNR values compared with previous sensors when expressed in neurons (Fig. 2c,d and Supplementary Table 1).

Our sensors also maintained the pharmacological specificity of their respective parent receptors. For example, application of the D_1R-specific and D_2R-specific antagonists SCH-23390 (SCH) and eticlopride, respectively, eliminated the corresponding sensors' response to DA (Fig. 2e and Extended Data Fig. 2); both D_1R-specific and D_2R-specific antagonists inhibited rDA2m and rDA2h (Fig. 2e and Extended Data Fig. 2b–d), possibly due to low sequence homology with human D_2R. Moreover, these sensors exhibited minimal response to a variety of other neurochemicals and transmitters. Importantly, despite the structural similarity between DA and norepinephrine (NE), our optimized sensors were approximately 7–80-fold more sensitive to DA than NE depending on the cell type (Fig. 2f and Extended Data Fig. 2).

Next, we measured the kinetics of our DA sensors using rapid line-scanning confocal microscopy. We locally applied DA or sensor antagonist to measure the time constant of both the signal rise (τ_{on}) and the signal decay (τ_{off}), respectively. Our analysis revealed τ_{on} values of approximately 80 ms for all DA sensors, and τ_{off} values ranging from 0.6 s to 3 s based on differences in each sensor's affinity (Extended Data Fig. 3 and Supplementary Table 1).

We investigated whether our red-shifted DA sensors are photoactivated by blue light, as shown previously for the cpmApple-based red calcium indicator jRGECO1a (refs. 22,29). Bursts of 488-nm blue light had no impact on the fluorescence of the rDA1m and rDA2 sensors (Fig. 2g and Supplementary Table 1), promising compatibility with blue-light-activated optogenetic actuators. However, similar to jRGECO1a, RdLight1 and rDA3 sensors displayed blue-light-induced photoactivation, causing a transient increase in fluorescence (Fig. 2g and Supplementary Table 1). Furthermore, the DA-induced increase in fluorescence remained stable for up to 2 h in the continuous presence of 100 μM DA, with minimal arrestin-mediated internalization or desensitization (Fig. 2h and Supplementary Fig. 3), making these sensors suitable for long-term monitoring of dopaminergic activity.

We then used the luciferase complementation assay[30] and the Tango assay[31] to examine the sensors' coupling to G-protein- and β-arrestin-mediated signaling, respectively. We found that wild-type receptors showed robust coupling in both assays, whereas all DA sensors failed to engage these GPCR-mediated downstream pathways (Fig. 2i,j), suggesting their expression likely has no impact on cellular physiology.

Imaging DA dynamics in acute brain slices

Using two-photon imaging, we next assessed the sensitivity of the gDA3m and rDA3m sensors in reporting endogenous DA release in acute brain slices. We injected adeno-associated virus (AAV) expressing either gDA3m or rDA3m into the NAc and then prepared acute brain slices 2 weeks later (Fig. 3a,b). Electrical stimuli applied at NAc at 20 Hz induced robust transient increases in fluorescence, and the amplitude of the peak response increases with increasing numbers of stimuli. Notably, application of the D_1R-selective antagonist SCH eliminated the stimulus-evoked response, confirming the specificity of sensor signals. Consistent with our results in cultured cells, both gDA3m and rDA3m exhibited significantly improved sensitivities and responses compared with the previous-generation sensors ($P = 0.0076$ between gDA3m and gDA2m, $P = 0.0008$ between rDA3m and rDA1m, two-tailed t-test; Fig. 3c–e).

Because the fluorescence of the D_1R-based gDA3m sensor is not affected by D_2R-specific compounds (Fig. 3f), we examined the effect of D2 autoreceptor activity on DA release in slices expressing the D_1R-based gDA3m sensor. Activation of endogenous D_2Rs by the D2-specific agonist quinpirole decreased the stimulus-evoked change in gDA3m fluorescence (Fig. 3g,h), reflecting presynaptic inhibition via D2 autoreceptors; this decrease was reversed by the addition of D_2R antagonist sulpiride, and adding the D_1R-specific antagonist SCH abolished the stimulation-evoked response (Fig. 3g,h).

https://doi.org/10.1038/s41592-023-02100-w

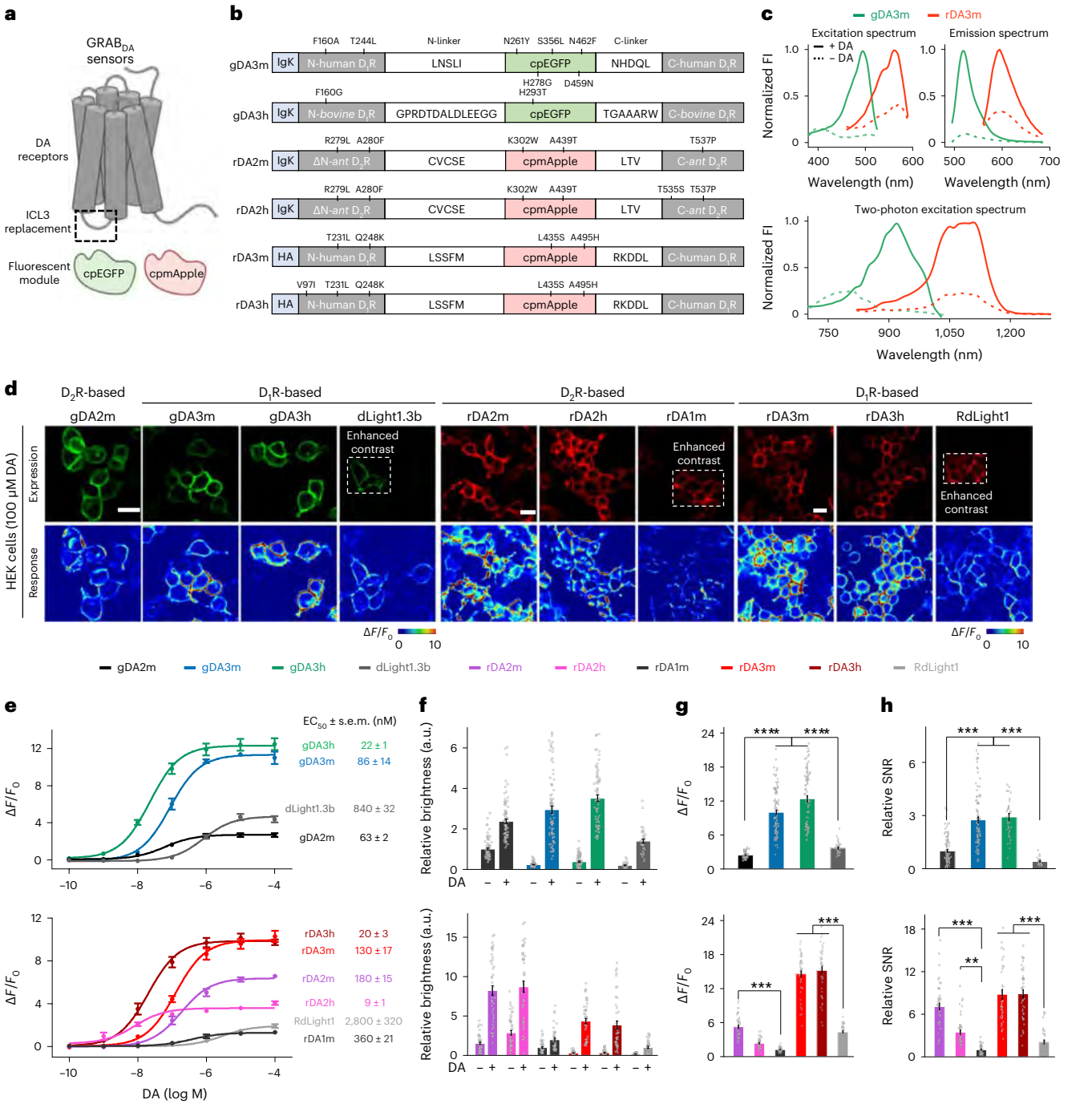

Fig. 1 | Development and performance of improved dual-color GRAB$_{DA}$ sensors. a, Schematic illustration showing the principle of next-generation DA sensors. **b**, Schematics of improved GRAB$_{DA}$ sensors. Mutations are indicated with respect to wild-type receptors and fluorescent proteins. Immunoglobulin κ-chain (Igk) leader sequenceor histamine (HA), N terminus leader sequence. **c**, Spectral profiles of GRAB$_{DA}$ sensors. One-photon excitation (top-left), emission (top-right) and two-photon excitation (bottom) spectra of indicated sensors with (dashed lines) or without (continuous lines) DA are shown. **d**, Representative images showing sensor expression (top) and fluorescence response to 100 μM DA (bottom) of indicated sensors. Scale bar, 20 μm. **e**, Titration DA curves of indicated sensors on HEK293T cells. Apparent EC$_{50}$ values are defined as the concentration of half-maximal fluorescence changes (max $\Delta F/F_0$), mean ± s.e.m. n = 4, 7, 10, 8, 7, 6, 6, 12, 12 and 12 wells for gDA3m, gDA3h, gDA2m, dLight1.3b, rDA2m, rDA2h, rDA1m, rDA3m, rDA3h and rDA3m, respectively, with an average of 400 cells per well. **f**, Group summary of brightness (relative to gDA2m and rDA1m, respectively) of indicated sensors before and after 100 μM DA addition. n = 90/5 (90 cells from 5 separate experiments), 81/5, 88/5, 36/3, 45/3, 45/3, 45/3, 45/3, 45/3 and 38/3 for gDA3m, gDA3h, gDA2m, dLight1.3b, rDA2m, rDA2h, rDA1m, rDA3m, rDA3h and RdLight1, respectively. **g**, Group summary of maximal $\Delta F/F_0$ of indicated sensors in response to 100 μM DA. n = 61/7, 102/10, 91/9, 35/3, 45/3, 45/3, 45/3, 45/3, 45/3, 38/3 for gDA3m, gDA3h, gDA2m, dLight1.3b, rDA2m, rDA2h, rDA1m, rDA3m, rDA3h and RdLight1, respectively, mean ± s.e.m. One-way ANOVA with post hoc Tukey's test was performed. $P = 1 \times 10^{-8}$ between gDA3m and gDA2m, or dLight1.3b; $P = 1 \times 10^{-8}$ between gDA3h and gDA2m, or dLight1.3b; $P = 1 \times 10^{-9}$ between rDA2m and rDA1m; $P = 1 \times 10^{-9}$ between RdLight1 and rDA3m, or rDA3h. **h**, Group summary of SNR (relative to gDA2m and rDA1m, respectively) of indicated sensors. n = 95/5, 40/3, 96/5, 31/3, 45/3, 45/3, 45/3, 45/3, 45/3, 38/3 for gDA3m, gDA3h, gDA2m, dLight1.3b, rDA2m, rDA2h, rDA1m, rDA3m, rDA3h and RdLight1, respectively, mean ± s.e.m. One-way ANOVA with post hoc Tukey's test was performed. $P = 1 \times 10^{-8}$ between gDA3m and gDA2m, or dLight1.3b; $P = 1 \times 10^{-8}$ between gDA3h and gDA2m, or dLight1.3b; $P = 0.0016$ between rDA2h and rDA1m; $P = 1 \times 10^{-9}$ between rDA2m and rDA1m; $P = 1 \times 10^{-9}$ between RdLight1 and rDA3m, or rDA3h. EC$_{50}$, half-maximum effective concentration; FI, fluorescence intensity.

https://doi.org/10.1038/s41592-023-02100-w

To measure DA release in both midbrain DA neuron cell bodies and terminals, we injected AAV expressing gDA3m into the substantia nigra pars compacta (SNc) driving expression in both regions, and prepared acute brain slices (Fig. 3i). Low-frequency stimulation (0.33 Hz) elicited time-locked transient increases in fluorescence in both the striatum and SNc. A 40-Hz train of five pulses induced a large transient increase in fluorescence, with a slower signal decay in the SNc compared with the striatum (Fig. 3k). We then conducted line-scan

https://doi.org/10.1038/s41592-023-02100-w

Fig. 2 | Characterization of GRAB$_{DA}$ sensors in cultured cells. a, Representative images of gDA3m- or rDA3m-expressing neurons. Scale bars, 100 μm (left) and 20 μm (right). **b**, Representative images showing expression and fluorescence response of indicated sensors in neurons. Scale bar, 50 μm. Similar results were observed in more than 30 cells. **c**, Titration DA curves (left) and group summary of peak response (top-right) and relative SNR (bottom-right) of indicated green sensors in neurons. Left, $n = 60, 60, 120, 60$ neurons for gDA2m, gDA3m, gDA3h and dLight1.3b, respectively; right, $n = 130, 175, 200, 80$ neurons, mean ± s.e.m. One-way ANOVA, post hoc Tukey's test: for both response and SNR, $P = 5 \times 10^{-10}$ between gDA3m and gDA2m, or dLight1.3b; $P = 5 \times 10^{-10}$ between gDA3h and gDA2m, or dLight1.3b. **d**, Similar to **c** except for red sensors. Left, $n = 30$ neurons for each sensor; right, $n = 60$ neurons for each, mean ± s.e.m. One-way ANOVA, post hoc Tukey's test: response, $P = 1 \times 10^{-9}$ between rDA2h and rDA1m; $P = 1 \times 10^{-11}$ between rDA2m and rDA1m; $P = 1 \times 10^{-11}$ between RdLight1 and rDA3m, or rDA3h; SNR, $P = 0.0006$ between rDA2h and rDA1m; $P = 1 \times 10^{-11}$ between rDA2m and rDA1m; $P = 1 \times 10^{-11}$ between RdLight1 and rDA3m, or rDA3h. **e**, Pharmacological specificity of indicated sensors in neurons. SCH, D_1R antagonist; eticlopride (Etic), D_2R antagonist; SKF-81297 (SKF), D_1R agonist; quinpirole (Quin), D_2R agonist; Glu, glutamate; GABA, γ-aminobutyric acid; L-Dopa, levodopa; 5-HT, serotonin; OA, octopamine; TA, tyramine. Antagonists were applied at 10 μM, others at 1 μM. $n = 4, 5, 3$ and 3 wells for gDA3m, gDA3h, rDA2m and rDA3m, respectively, with an average of 100 neurons per well, mean ± s.e.m. One-way ANOVA, post hoc Dunnett's test: gDA3m, $P = 0.0831$ between DA and DA + Etic; $P = 1.3 \times 10^{-13}$ between DA and others; gDA3h, $P = 0.2744, 0.0008$ between DA and DA + Etic, or SKF; $P = 1.0 \times 10^{-15}$ between DA and others; rDA2m, $P = 1.0 \times 10^{-13}$ between DA and others; rDA3m, $P = 0.8251, 0.9993$ between DA and DA + Etic, or SKF; $P = 4.0 \times 10^{-14}$ between DA and others. **f**, Titration curves of indicated sensors for the response to DA or NE in neurons. DA, $n = 45, 80, 60$ and 90 neurons from 3 experiments for gDA3m, gDA3h, rDA2m and rDA3m; NE, $n = 45, 120, 30$ and 60 neurons from 3 experiments for gDA3m, gDA3h, rDA2m and rDA3m, mean ± s.e.m. **g**, Representative traces (left) and group summary of $\Delta F/F_0$ (right) of indicated sensors upon blue-light illumination. $n = 71, 13, 17, 18, 14, 8, 8, 18, 16$ cells for jRGECO1a, rDA1m, rDA2m, rDA2h, rDA2mut, RdLight1, rDA3m, rDA3h and rDA3mut, respectively, mean ± s.e.m. One-way ANOVA, post hoc Dunnett's test: $P = 0.2726$ between jRGECO1a and D_1R-based red sensors; $P = 1 \times 10^{-15}$ between jRGECO1a and D_2R-based red sensors. **h**, Representative images (left) and quantification (right) of sensor fluorescence in response to 2-h application of 100 μM DA. Scale bar, 20 μm. $n = 3$ and 9 cultures for gDA3m and rDA3m, respectively, mean ± s.e.m. One-way ANOVA test was performed for each sensor among DA-containing groups: $P = 0.4375, 0.1895$ for gDA3m and rDA3m. **i**, Luciferase complementation assay for assessing G-protein coupling. Cells expressing mG$_{s/i}$ alone serve as the control. $n = 3$ cultures each, mean ± s.e.m. One-way ANOVA, post hoc Tukey's test: $P = 2 \times 10^{-8}$ between bD$_1$R and gDA3h; $P = 1 \times 10^{-8}$ between hD$_1$R and gDA3m; $P = 3 \times 10^{-7}$ between aD$_2$R and rDA2m, or rDA2h; $P = 0.92, 0.95$ between Gi-LgBit and rDA2m, or rDA2h; $P = 9 \times 10^{-7}, 5 \times 10^{-7}$ between hD$_1$R and rDA3m, or rDA3h; $P = 0.77, 0.99$ between Gs-LgBit and rDA3m, or rDA3h. **j**, Tango assay for assessing β-arrestin coupling. $n = 3$ cultures each, mean ± s.e.m. NA, not applicable. One-way ANOVA, post hoc Tukey's test: $P = 6 \times 10^{-6}$ between bD$_1$R and gDA3h; $P = 1 \times 10^{-8}$ between hD$_1$R and gDA3m; $P = 2 \times 10^{-7}, 3 \times 10^{-7}$ between aD$_2$R and rDA2m, or rDA2h; $P = 0.0002, 0.0002$ between hD$_1$R and rDA3m, or rDA3h. NS, not significant.

microscopy (2 ms per line) to analyze the kinetics. Our results revealed that the fluorescence increase upon high-frequency stimulation had a half-rise time (rise $t_{1/2}$) of 20 ± 10 ms (mean ± s.d.) and 22 ± 9 ms in the striatum and SNc, respectively; however, the fluorescence signal decayed more slowly to baseline in the SNc (decay $t_{1/2}$) than the striatum, with decay $t_{1/2}$ values of 209 ± 49 ms and 125 ± 32 ms, respectively (Fig. 3l). This temporal difference in DA signals may be attributed in part to differences in dopamine transporter (DAT) expression between the dorsal striatum and midbrain[32].

Validation of next-generation DA sensors in vivo

Next, we examined whether the increased sensitivity of our DA sensors might be suitable for recording in vivo DA release in the sparsely innervated mPFC. We therefore virally expressed the optogenetic tool ChrimsonR[33] in the ventral tegmental area (VTA) and either gDA3h or dLight1.3b in the mPFC; we then optically stimulated the VTA and measured the signal in the mPFC through fiber photometry (Extended Data Fig. 4a,b). We found that activating VTA neurons elicited robust, transient increases in fluorescence in the gDA3h-expressing mPFC, and this increase was blocked by SCH (Extended Data Fig. 4c–f). Besides, the gDA3h sensor had pulse-dependent responses to optogenetic stimulation, and a single light pulse was adequate to elicit a response; in contrast, activating VTA neurons had virtually no effect on dLight1.3b (Extended Data Fig. 4c–i), indicating that this previous-generation DA sensor lacks the sensitivity to detect in vivo DA release in the mPFC.

To assess the in vivo performance of our red-shifted GRAB$_{DA}$ sensors, we expressed either rDA3m or rDA3mut in the central amygdala, and the light-activated channel Channelrhodopsin-2 (ChR2) (ref. 34)

Fig. 3 | Ex vivo and in vivo validation of GRAB$_{DA}$ sensors. a, Schematic illustration depicting the experimental design for panels **b**–**e**. **b**, Representative images showing gDA3m or rDA3m expression in the NAc. Scale bar, 100 μm. Similar results were observed from more than four mice. **c**, Example fluorescence response to indicated electrical stimulation in the sensor-expressing brain slices. Dashed circles, ROIs used to analyze the responses. Scale bar, 100 μm. **d**, Representative traces (left) and group summary (right) of the change in gDA3m sensor fluorescence to electrical stimulation. Left, mean ± s.d. Right, mean ± s.e.m. $n = 8$ slices from 5 mice (8/5) for gDA3m. The inset shows quantification of the $\Delta F/F_0$ of indicated sensors to 1-pulse stimulation. Data were replotted from previous results of gDA2m (ref. 13). Two-tailed Student's t-test: $P = 0.0429$ for gDA3m, $P = 0.0076$ between gDA3m and gDA2m. **e**, Representative traces (left) and group summary (right) of the change in rDA3m sensor fluorescence to electrical stimulation. Left, mean ± s.d. Right, mean ± s.e.m. n = 5/4 for rDA3m. The inset shows quantification of the $\Delta F/F_0$ of indicated sensors to 1-pulse stimulation. Two-tailed Student's t-test: $P = 0.0138$ for rDA3m, $P = 0.0008$ between rDA3m and rDA1m. Data were replotted from previous results of rDA1m (ref. 13). **f**, Normalized fluorescence change in gDA3m to indicated compounds (1 μM). Sulpiride (Sulp), D_2R antagonist. $n = 3$ wells with 500–600 cells per well, mean ± s.e.m. One-way ANOVA, post hoc Dunnett's test: $P = 0.9813, 0.8848$ between DA and DA+Quin, or DA+Sulp. **g**, Representative pseudocolored images (top) and fluorescence response traces (bottom, mean ± s.d.) of gDA3m to electrical stimuli in indicated conditions (drugs in 1 μM). Yellow dashed line, electrode placement; dashed circles, ROIs. Scale bar, 100 μm. **h**, Group summary of fluorescence response of gDA3m to electrical stimulation either in artificial cerebrospinal fluid (ACSF) or with indicated drugs. $n = 6$ slices from 5 mice, mean ± s.e.m. One-way ANOVA, post hoc Tukey's test: $P = 0.0023$, $P = 0.9999$, $P = 0.0008$ between ACSF and Quin, Sulp or SCH; $P = 0.00231$ between Quin and Sulp. **i**, Schematic illustration depicting the experimental design of panels **j**–**l**. **j**, Representative images showing gDA3m expression in the striatum (top) and SNc (bottom) in the control condition (left) and upon stimulation (right). Scale bar, 5 μm. Yellow lines, line-scanning regions. Similar results were observed from more than five slices. **k**, Full-frame fluorescence response (relative to the peak of the first stimulation) to indicated electrical stimulations. $n = 6$ slices for striatum, $n = 9$ slices for SNc, mean ± s.e.m. **l**, Representative line-scan image in the striatum (top) and the SNc (bottom) and averaged normalized traces to multi-pulse stimulus. $n = 6$ areas for striatum and SNc, respectively, mean ± s.e.m. **m**, Schematic illustration depicting the experimental design for panels **n**–**q**. **n**, Histological verification of rDA2m expression in mPFC and NAc, and ChrimsonR expression in VTA. Dashed boxes, optical tracts. Scale bar, 1 mm. **o**, Representative traces of rDA2m signals in the mPFC (top) and NAc (bottom) during optogenetic stimulations. **p**, Average traces of sensor response in the mPFC (left) and NAc (right) to indicated optogenetic stimulation from a mouse, mean ± s.d. The length of blue lines indicates the duration of opto-stimulation. **q**, Group summary of peak response of indicated sensors to indicated optogenetic stimulation. $n = 3$ mice for rDA2m and rDA2mut, mean ± s.e.m. Two-tailed Student's t-test was performed between groups for 10-s opto-induced response. mPFC, $P = 0.0007$; NAc, $P = 0.0364$. 1m, rDA1m; 2m, gDA2m; 3m in **d**, gDA3m; 3m in **e**, rDA3m; 2PM, two-photon microscope.

https://doi.org/10.1038/s41592-023-02100-w

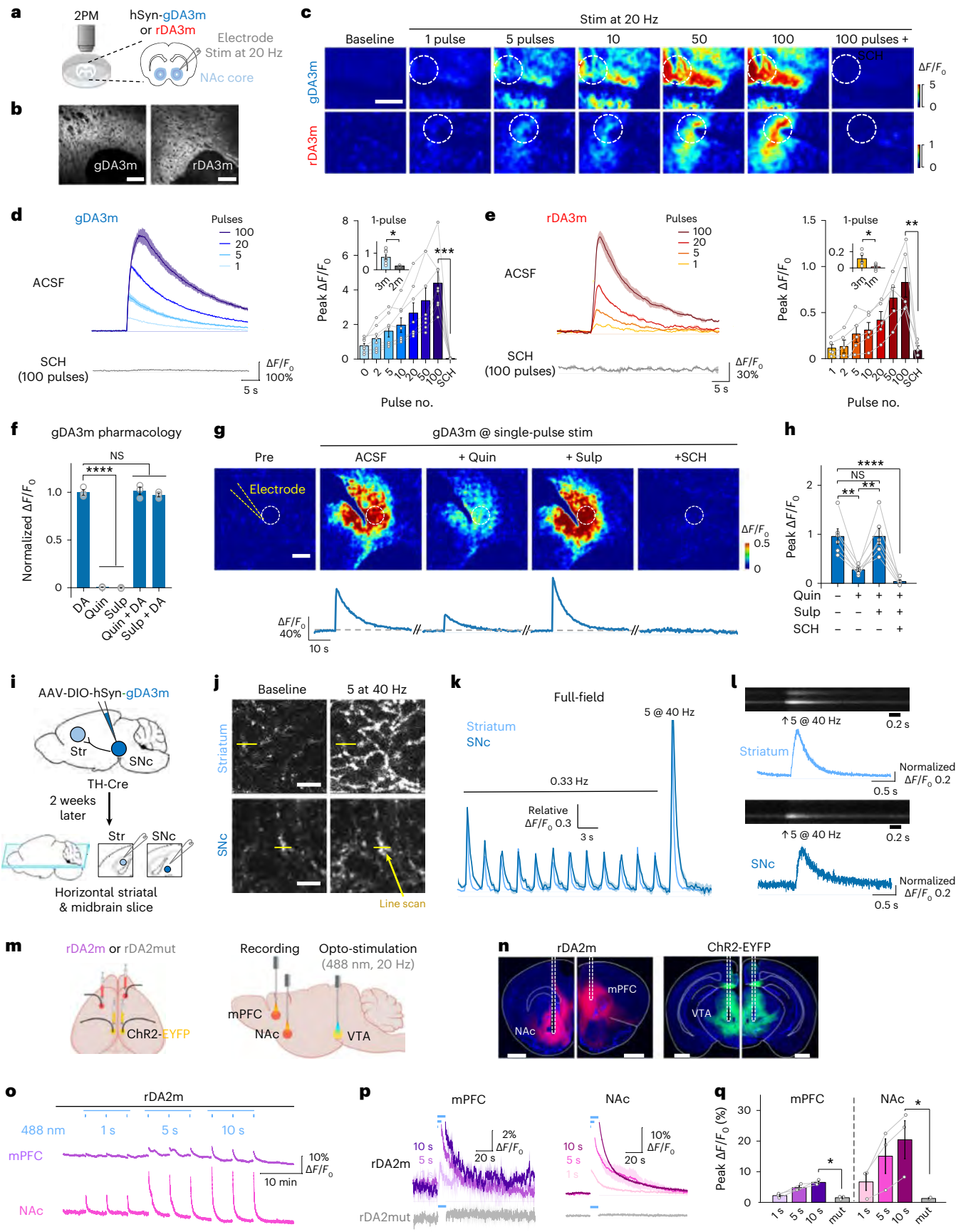

https://doi.org/10.1038/s41592-023-02100-w

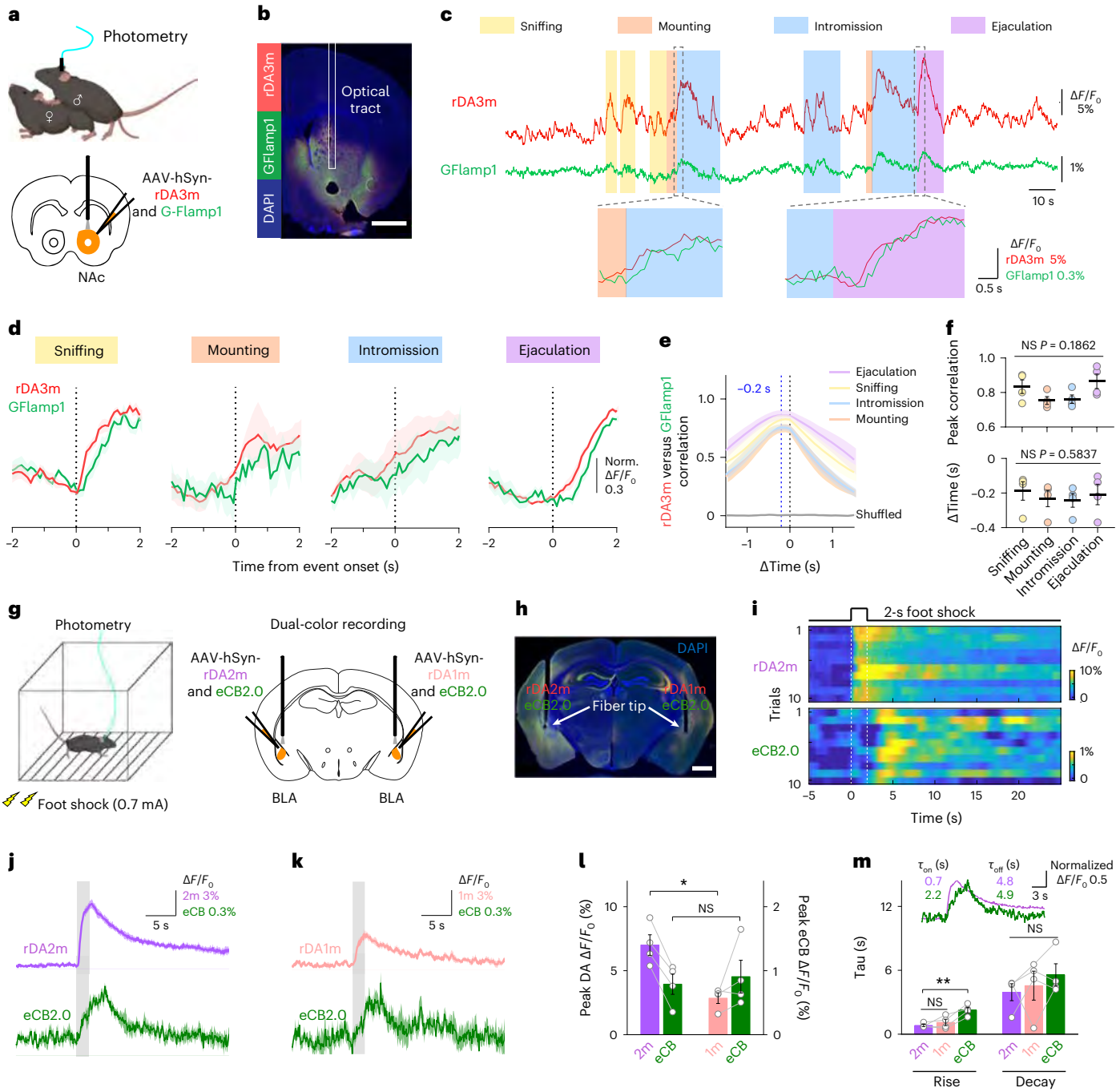

Fig. 4 | Multiplexed measurements of DA and other neurochemical signals during natural behaviors. a, Schematic illustration depicting the experimental design for panels **b**–**f**. **b**, Histological verification of rDA3m and G-Flamp1 expression in NAc. DAPI, 4,6-diamidino-2-phenylindole. Scale bar, 1 mm. **c**, Example traces (top) and magnified traces of rDA3m (red) and G-Flamp1 (green) signals simultaneously measured during the indicated mating stages. **d**, Group-averaged rDA3m and G-Flamp1 fluorescence aligned to event onset for all mice. The signals were normalized to respective maxima and minimum. $n = 4$ mice, mean ± s.e.m. **e**, Cross-correlation between simultaneously recorded rDA3m and G-Flamp1 signals during indicated stages and of shuffle group. $n = 4$ mice, mean ± s.e.m. **f**, Group summary of peak correlation coefficient (top) and time lag of cross-correlation peak (bottom) between rDA3m and G-Flamp1 signals across mating stages. $n = 4$ mice, mean ± s.e.m. One-way ANOVA with post hoc Tukey's test was performed. **g**, Schematic illustration depicting the experimental design for panels **g**–**k**. **h**, Histological verification of rDA2m and eCB2.0 expression (left) and rDA1m and eCB2.0 expression (right) in BLA. Scale bar, 1 mm. **i**, Pseudocolored fluorescence responses of rDA2m and eCB2.0 measured in the BLA to ten consecutive foot shocks. **j**, Average traces of the change in rDA2m (top) and eCB2.0 (bottom) fluorescence from a mouse. The gray-shaded area indicates the application of electrical foot shock, mean ± s.d. **k**, Same as **h** with simultaneously recorded contralateral rDA1m and eCB2.0 signals. **l**, Group summary of the peak change in fluorescence of indicated sensors to foot shock. $n = 4$ mice, mean ± s.e.m. Paired two-tailed Student's t-test was performed. $P = 0.0390$ between rDA2m and rDA1m; $P = 0.7019$ between eCB2.0 groups. **m**, Summary of rise and decay time constants measured for the fluorescence change of indicated sensors to foot shock. The inset shows the example average trace of rDA2m and eCB2.0 signals that were normalized to respective maxima and minimum. $n = 4$ mice, mean ± s.e.m. One-way ANOVA with post hoc Dunnett's test was performed. Rise time, $P = 0.5742$ and 0.0087 between rDA2m and rDA1m, or eCB2.0. Decay time, $P = 0.2180$ for all groups.

https://doi.org/10.1038/s41592-023-02100-w

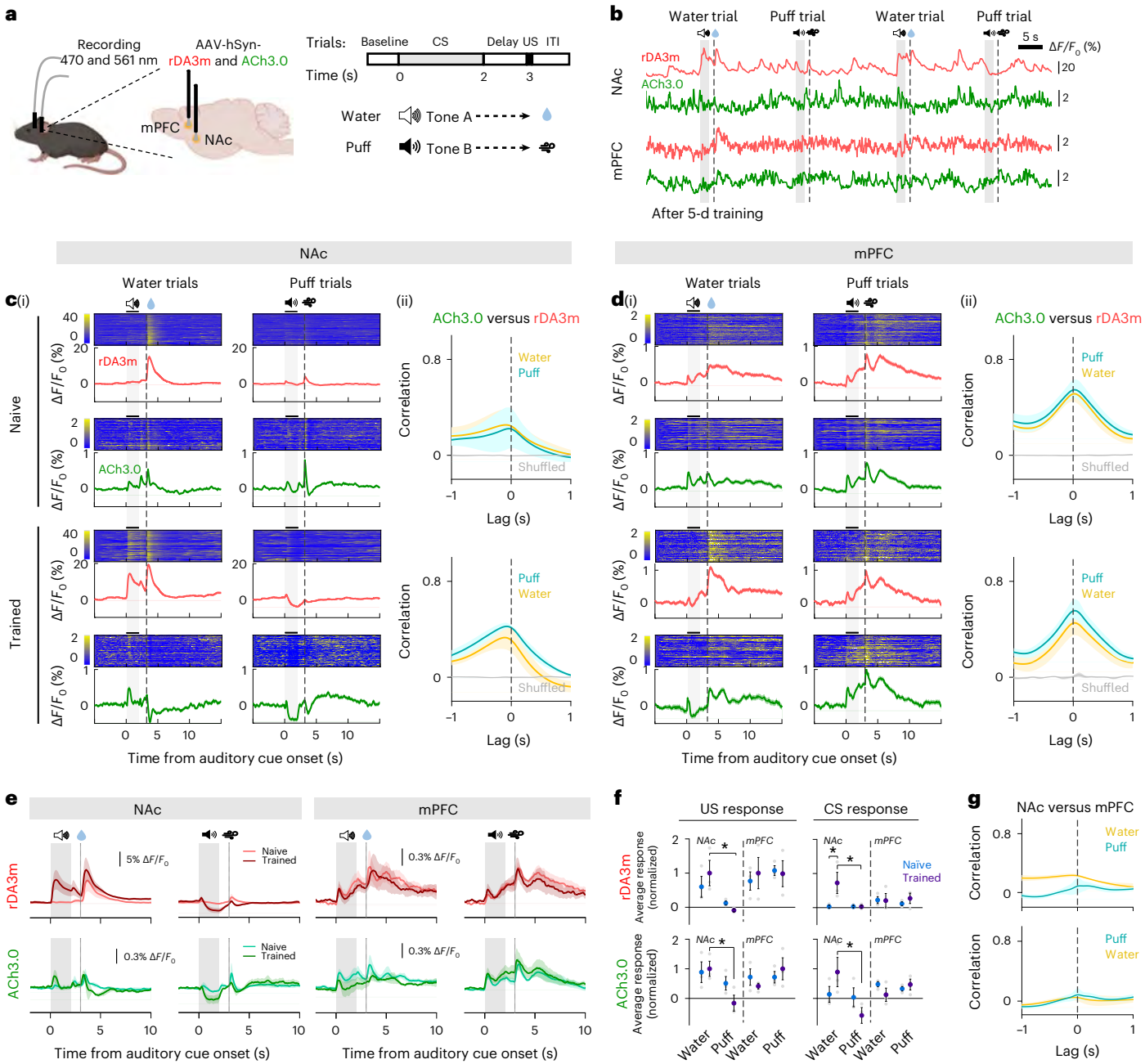

Fig. 5 | DA and ACh signals in mouse NAc and mPFC during an auditory Pavlovian conditioning task. a, Schematic illustration depicting experimental design for panels **b**–**g**. **b**, Example traces of rDA3m (red) and ACh3.0 (green) signals ($\Delta F/F_0$) simultaneously measured in the NAc (top) and mPFC (bottom) from a trained mouse during four consecutive trials. The audio, water and puff delivery are indicated above. **c**, Representative time-aligned pseudocolored images and averaged traces (mean ± s.e.m.) of rDA3m and ACh3.0 fluorescence from a mouse in naive (top) and trained (bottom) state (**c**(i)). The gray-shaded area indicates the application of audio. The dashed line indicates the delivery of water or puff. Session-wide correlation between rDA3m and ACh3.0 signals across naive (top) and trained sessions (bottom) (**c**(ii)). $n = 3$ mice. **d**, The same as **c** with simultaneously recorded rDA3m and ACh3.0 signals in the mPFC. **e**, Group-averaged rDA3m (top) and ACh3.0 (bottom) fluorescence in the NAc (left) and mPFC (right) for all mice under naive and trained states. Water or puff sessions are indicated above. $n = 3$ mice. **f**, Group analysis of the normalized average change of rDA3m (top) and ACh3.0 (bottom) signals to US (left) and CS (right) in different sessions. The average response was calculated as the average $\Delta F/F_0$ in the 1 s after the behavior onset. The gray points indicate data from individual animals; average and s.e.m. are shown by data points with state-represented color. $n = 3$ mice. Two-way ANOVA with post hoc Sidak's test was performed between water and puff sessions and between naive and trained states. Responses in the trained mice NAc, $P = 0.0145$ (rDA3m-US), 0.0287 (rDA3m-CS), 0.0371 (ACh3.0-US), 0.0356 (ACh3.0-CS) between water and puff trials; rDA3m water trial CS response in the NAc, $P = 0.0290$ between naive and trained. **g**, Session-wide cross-correlation between rDA3m (top) or ACh (bottom) signals recorded in the NAc and mPFC. $n = 3$ mice. CS, conditional stimulus; ITI, inter-trial interval; US, unconditional stimulus.

in the VTA (Extended Data Fig. 5a,b). We found that activating VTA neurons induced robust, transient and pulse number-dependent increases in rDA3m fluorescence. These responses were eliminated by SCH administration and were absent in mice expressing the DA-insensitive rDA3mut sensor (Extended Data Fig. 5c–e). Additionally, rDA2m expressing in both the mPFC and the NAc of anesthetized animals also reported optogenetic activation-induced DA release, with larger signals in the NAc than the mPFC (Fig. 3m,n and Extended Data Fig. 5f,g);

in contrast, no signal was detected with the DA-insensitive rDA2mut sensor (Fig. 3o–q and Extended Data Fig. 5h).

To further compare the performance of the next-generation DA sensors with the reported GRAB variants, we measured the DA dynamics in the NAc of water-restricted mice when receiving water rewards (Extended Data Fig. 6a–c). We found that unexpected water delivery induced significantly larger fluorescence increases in both gDA3m and rDA3m compared with gDA2m and rDA1m, respectively ($P = 0.0095$ between gDA3m and gDA2m, $P = 0.0285$ between rDA3m and rDA1m, two-tailed Mann–Whitney U-test; Extended Data Fig. 6d–i). With enhanced SNR, gDA3m and rDA3m effectively distinguish variations in reward size (Extended Data Fig. 6j). We also compared rDA3m and RdLight1 expressing in opposite sides of the NAc core with bilateral fiber photometry recordings (Extended Data Fig. 6k,l). The rDA3m sensor consistently showed substantially higher fluorescence changes than RdLight1 across all water-rewarded sessions (Extended Data Fig. 6m,n). Taken together, our DA probes exhibited enhanced sensitivity and precision of DA detection in vivo.

To examine the DA/NE selectivity of our sensors in vivo, we expressed them in the mPFC, a region receiving both dopaminergic and noradrenergic innervations, and used fiber photometry to monitor sensor fluorescence during NE elevation (Extended Data Fig. 7). In contrast to the NE2m sensor[18], which showed significant fluorescence increases with the NET blocker desipramine-induced NE elevation[35] ($P = 0.0012$, paired two-tailed t-test; Extended Data Fig. 7a), neither rDA3m nor gDA3h showed detectable changes during despramine treatment, although they robustly reported optogenetically evoked DA transients in the mPFC (Extended Data Fig. 7b–e). These results suggest that rDA3m and gDA3h exhibit good selectivity for DA at physiologically relevant concentrations, even in the mPFC where DA and NE coexist. Furthermore, no behavioral differences were found in multiple DA-related behavioral tests between rodents expressing control fluorescent protein or DA sensors in the NAc (Extended Data Fig. 8), suggesting no apparent impact of sensor expression on DA-related animal behaviors.

In vivo dual-color imaging of DA and other neurochemicals

Exploiting the spectral compatibility of our red-shifted DA sensors with green fluorescent sensors, we simultaneously monitored multiple signaling events in the same location. The NAc plays a key role in reward processing. Therefore, we measured extracellular DA and intracellular cyclic AMP (cAMP), the downstream messenger activated by DA receptors and a point of convergence for GPCR signaling[36,37]. We expressed both rDA3m and the green fluorescent cAMP indicator G-Flamp1 (ref. 38) in the NAc of male mice and measured both signals during mating (Fig. 4a,b). We found that the fluorescence of rDA3m and G-Flamp1 measured in the NAc increased while the male was sniffing and mounting the female, and during intromission and ejaculation (Fig. 4c). Notably, rDA3m signals preceded G-Flamp1 signals by around 200 ms during all mating stages (Fig. 4d,f). Moreover, cross-correlation analysis revealed a close correlation between DA signals and intracellular cAMP levels (Fig. 4e,f).

As both DA and endocannabinoid (eCB) systems in the basolateral amygdala (BLA) were reported to participate in anxiety and fear formation[39], we next expressed rDA2m and the green eCB indicator eCB2.0 (ref. 40) in the BLA of one hemisphere and measured both signals while applying mild foot shocks. As a control, we expressed and measured rDA1m and eCB2.0 in the other hemisphere (Fig. 4g,h). We found that rDA2m and eCB2.0 had reproducible, time-locked transient increases in fluorescence upon foot shock; notably, rDA2m generated approximately twice the signal of rDA1m, whereas eCB2.0 signals were similar between hemispheres (Fig. 4i–l). We also examined the signal kinetics, and found similar τ_{off} rates for DA and eCB (around 4–5 s) but significantly faster τ_{on} rate for DA (~0.8 s) compared with eCB (~2.2 s), with no significant difference between rDA2m and rDA1m ($P = 0.0087$ between rDA2m and eCB2.0, $P = 0.5742$ between rDA3m and rDA1m, one-way analysis of variance (ANOVA) post hoc Dunnett's test; Fig. 4m).

DA and acetylcholine release during a Pavlovian conditioning task

Dopaminergic signaling is vital for reinforcing learning through the mesocorticolimbic system[41]. External rewards also elicit characteristic changes in acetylcholine (ACh) levels, facilitating learning and motivating action[42]. However, the relationship between DA and ACh release, as well as their dynamics during reinforcement learning, remained unclear. We therefore coexpressed rDA3m and the green fluorescent ACh sensor ACh3.0 (ref. 43) in the NAc and mPFC, and measured DA and ACh release during auditory Pavlovian conditioning tasks (Fig. 5a,b). Initially, rDA3m primarily responded to the rewards, while ACh3.0 responded to both rewards and punishments, with minimal response to auditory cues (Fig. 5c). After 5 d of training, the rDA3m and ACh3.0 signals in the NAc increased in response to the water-predicting tone, but decreased for the punishment-related tone, whereas their responses to actual reward or punishment remained in the current paradigm (Fig. 5c,e,f). The development of excitatory responses to the reward cue and inhibitory responses to the punishment cue is consistent with the so-called reward-prediction-error theory[41]. rDA3m and ACh3.0 signals in the mPFC increased in response to both cue types and the outcomes of both valences in naive mice, with no signal shift after training (Fig. 5d–f). Furthermore, DA and ACh signals were positively correlated during reward and punishment trials in both brain regions (Fig. 5c,d), indicating similar upstream regulation or local neuromodulatory effect[17] in these two regions. However, signals were uncorrelated between two brain areas (Fig. 5g), suggesting a heterogeneity of neurotransmission in the mesocorticolimbic system. As a control, we found that systemic administration of SCH effectively reduced the rDA3m signal without affecting the ACh3.0 signal (Extended Data Fig. 9).

Fig. 6 | Spatially resolved heterogenous cortical DA dynamics in mice. **a**,**b**, Schematic illustration depicting virus injection and head-fixed two-photon imaging in the mouse motor cortex. **a**, Example image showing gDA3h expression in the M1/M2 in a coronal brain slice. Scale bar, 500 µm. **b**, Representative in vivo two-photon image of layer 2/3 in the M1/M2 showing gDA3h fluorescence. Scale bar, 100 µm. **c**, Schematic cartoon illustrating forced running experiments (**c**(i)), representative pseudocolored response images (**c**(ii)) and traces measured at indicated ROIs (white squares) during three trials (**c**(iii)) in mice expressing gDA3h (top) or mEGFP (bottom). Scale bar, 50 µm. **d**,**e**, Similar to **c** except mice were subjected to tail shock (**d**) or audio (**e**). Two-photon imaging was performed in the same region across behaviors. **f**, Group summary of the peak fluorescence changes of gDA3h and mEGFP to indicated stimulus. $n = 5$ and 4 mice for gDA3h and mEGFP, mean ± s.e.m. Two-tailed Student's t-test: running, $P = 4 \times 10^{-5}$; shock, $P = 0.0017$. **g**, Group summary of the rise and decay time constant of gDA3h signals to forced running and tail shock. $n = 5$ mice, mean ± s.e.m. **h**, Example image showing the spatial responding pattern to forced running, tail shock, merge and ROI selection. **i**, Hierarchical clustering of ROI-specific responses to running and shock from a mouse. ROIs are indicated in **h**. **j**, Same to **h** with data from another two mice. **k**, Population data showing hierarchical clustering of ROI-specific response. $n = 91$ ROIs from 5 mice. **l**,**m**, Average (bold lines) and individual (thin lines) traces (**l**) and quantifications of response amplitudes (**m**) from ROIs within each cluster in **k** during different behaviors. The black lines indicate the application of indicated stimulus. $n = 26$, 24, 21 and 20 ROIs from 5 mice for each cluster, mean ± s.e.m. One-way ANOVA, post hoc Tukey's test: forced running, $P = 0.0128$, 0.0585 between none and shock, or between running and both; tail shock, $P = 0.9989$, 0.6474 between none and running, or between shock and both; audio, $P = 0.0766$ among clusters. **n**, Percentage of area that was responsive to the indicated stimulus as in **h**. **o**, Venn diagram of the imaged motor cortex area that was responsive to the indicated stimulus. $n = 5$ mice. A, anterior; L, lateral; M, medial; P, posterior.

https://doi.org/10.1038/s41592-023-02100-w

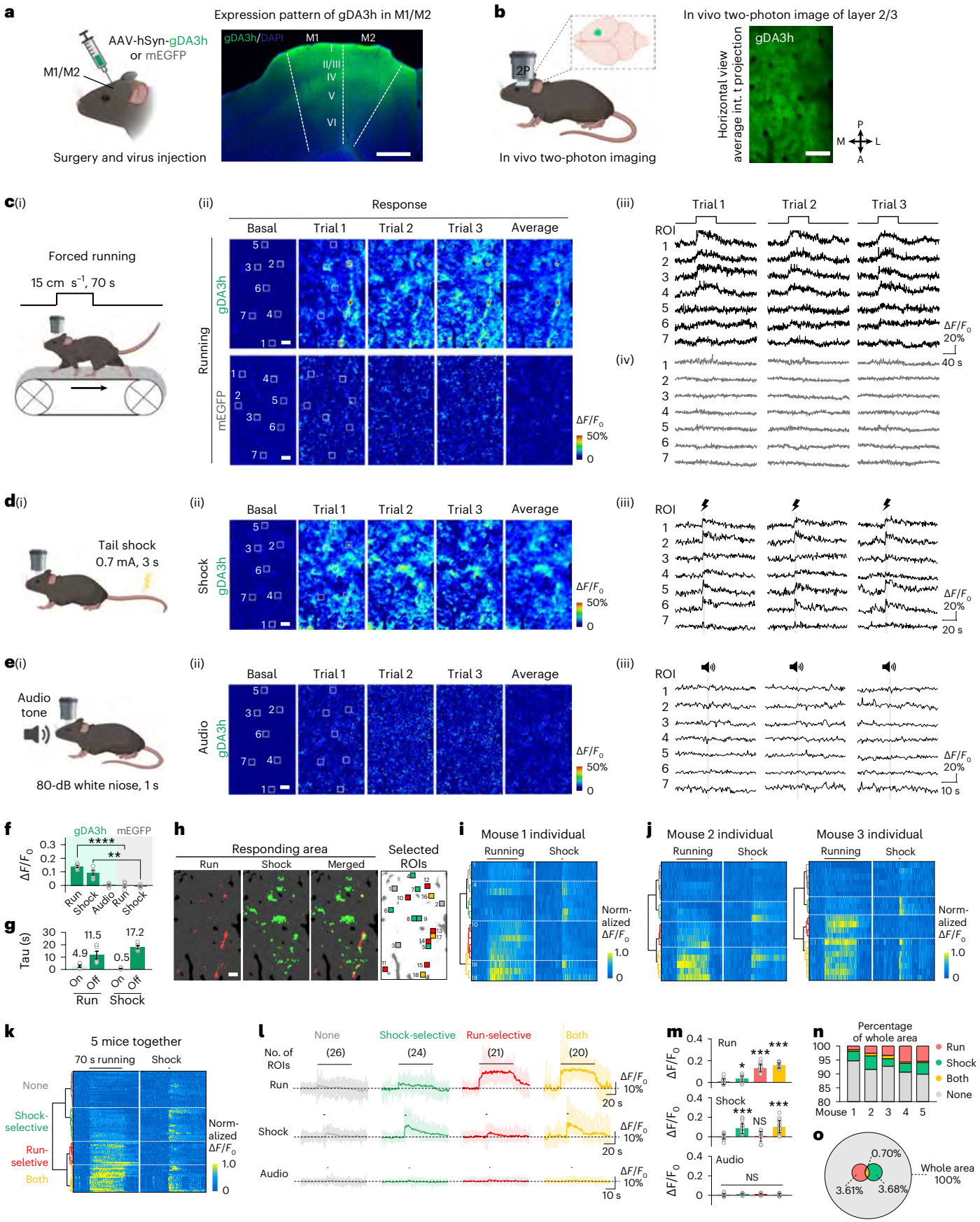

Spatially resolved imaging of cortical DA release

The cortex receives distinct dopaminergic signals from the SNc and VTA[3,44]. To test whether our high-affinity gDA3h sensor enables monitoring of behavior-related changes in cortical DA levels with high spatiotemporal precision, we expressed gDA3h in the M1/M2 motor cortex (Fig. 6a) and performed head-fixed in vivo two-photon imaging (Fig. 6b). During imaging, the mouse was placed on a treadmill and gDA3h fluorescence was measured in response to a 70-s bout of forced running (Fig. 6c), an electrical tail shock (Fig. 6d) or an auditory stimulus (Fig. 6e). We observed a robust, rapid, reproducible increase in gDA3h fluorescence aligned to the onset of forced running and tail shock, but not in response to the auditory stimulus (Fig. 6c–g). Similar results were obtained with gDA3m, while dLight1.3b lacked the sensitivity to capture these mild changes in DA (Extended Data Fig. 10). A control group expressing membrane-targeted EGFP (mEGFP) showed no fluorescence response (Fig. 6c,g and Extended Data Fig. 10). We then examined the spatial patterns of DA release during forced running and tail shock on a trial-by-trial basis; we observed distinct patterns during running and shock (Fig. 6c–e). Consistent with this observation, further hierarchical cluster analysis identified four distinct categories of cell-sized regions of interest (ROIs) (Fig. 6h–j), which was consistently observed in all tested animals (Fig. 6k–m). A small subset of regions (representing 0.7% of the entire area) exhibited DA increases during both running and shock, while 3.61% and 3.68% of the entire area were primarily associated with running or shock, respectively (Fig. 6n,o). Collectively, our gDA3h sensor allows the mapping of spatially and functionally diverse patterns of DA release in the motor cortex with subsecond resolution.

Discussion

Here we used rational design to develop a third-generation series of highly sensitive and selective DA sensors for in vivo multiplex imaging. Considering the current imbalance in availability of red versus green sensors, in combination with other recently developed optical sensors (for example, cAMP, eCB and ACh sensors), the improved red DA sensors expand the variety of signaling events that can be studied simultaneously for end users.

With combined use of DA and cAMP sensors, our data suggest a positive correlation between signals in the NAc of male mice during mating behaviors. However, it is important to note that our observation was based on photometry-recorded net signals without differentiating cell type specificity. To fully understand the cAMP signaling in distinct medium spiny neuron populations in the NAc[45], further studies using fiber photometry recording or single-cell-resolution imaging techniques with G-Flamp1-labeled D1 or D2 medium spiny neurons is warranted.

Although several fluorescent DA sensors have been developed using the GPCR-based strategy, they often lack sufficient sensitivity to monitor mild DA release. Our highly sensitive DA sensors overcome this limitation, enabling in vivo DA imaging in several brain regions such as the amygdala and cortex. Importantly, our simultaneous recordings of localized DA release in the NAc and mPFC revealed asynchronous DA release from distinct axonal termini. Specifically, in Pavlovian conditioning, NAc DA signals were consistent with the theory of prediction-error, while mPFC DA signals mirrored reported cortical dopaminergic activity in stimulus discrimination[46], together suggesting functional heterogeneity within DA neurons. In addition, even within a given region such as the motor cortex, our two-photon imaging of gDA3h revealed behaviorally related, spatially resolved heterogeneity in cortical dopaminergic signaling.

As no one sensor fits all conditions, end users should first determine which sensor is optimally matched with their imaging conditions and experiments to maximize signals. Firstly, for imaging DA in brain regions with moderate to high DA levels, medium-affinity DA sensors such as gDA3m and rDA3m would be the first choices. These sensors offer the highest fluorescence changes, ensuring excellent SNR and a broad concentration range for DA detection. Meanwhile, higher affinity sensors such as gDA3h and rDA3h are ideal for sparsely innervated brain regions, as they are sensitive to subtle DA level changes. Secondly, one should also consider the tradeoffs concerning sensor kinetics. The medium-affinity sensors with faster off kinetics provide good balance between SNR and kinetics, and can resolve multiple signals within seconds or subseconds, thus are well-suited for monitoring DA dynamics during rapidly changing events. Another important factor to consider is the color of sensor spectra when multiplexing DA imaging with other neurochemical signals or optogenetics. Both green and red sensors are compatible with two-color imaging given their orthogonal spectra profiles. The green set is compatible with red-shifted optogenetics, and the D2-based red ones are insensitive to blue excitation light and therefore compatible with blue-light-excited opsins. Note that despite a blue-light activation of rDA3 series reported in vitro, they experienced minimal interference from blue excitation light in vivo. End users could further minimize potential crosstalk by using separate excitation steps, and validate the signal specificity by adding proper controls (for example, DA-insensitive sensors). To be noted, a potential caveat of DA imaging in the cortex is the possibility of cross-detection of NE, even with the improved sensors that have high DA/NE selectivity in vivo. This issue may vary in different behavioral contexts, and interference from NE cannot be entirely ruled out in cases of exceptionally high NE levels. Given the coexistence of DA and NE in many regions, it is crucial to develop next-generation $GRAB_{DA}$ sensors with nonoverlapping DA and NE specificity.

In combination with multicolor fluorescence imaging of other signaling events, our series of DA sensors enable functionally mapping neurochemical activity and will contribute to a deeper understanding of the complexity of the dopaminergic system.

Online content

Any methods, additional references, Nature Portfolio reporting summaries, source data, extended data, supplementary information, acknowledgements, peer review information; details of author contributions and competing interests; and statements of data and code availability are available at https://doi.org/10.1038/s41592-023-02100-w.

References

1. Aransay, A., Rodríguez-López, C., García-Amado, M., Clascá, F. & Prensa, L. Long-range projection neurons of the mouse ventral tegmental area: a single-cell axon tracing analysis. *Front. Neuroanat.* **9**, 59 (2015).
2. Slaney, T. R., Mabrouk, O. S., Porter-Stransky, K. A., Aragona, B. J. & Kennedy, R. T. Chemical gradients within brain extracellular space measured using low flow push-pull perfusion sampling in vivo. *ACS Chem. Neurosci.* **4**, 321–329 (2013).
3. Björklund, A. & Dunnett, S. B. Dopamine neuron systems in the brain: an update. *Trends Neurosci.* **30**, 194–202 (2007).
4. Klaus, A., Alves da Silva, J. & Costa, R. M. What, if, and when to move: basal ganglia circuits and self-paced action initiation. *Annu. Rev. Neurosci.* **42**, 459–483 (2019).
5. Wise, R. A. Dopamine, learning and motivation. *Nat. Rev. Neurosci.* **5**, 483–494 (2004).
6. Goldman-Rakic, P. S. The cortical dopamine system: role in memory and cognition. *Adv. Pharmacol.* **42**, 707–711 (1998).
7. Ott, T. & Nieder, A. Dopamine and cognitive control in prefrontal cortex. *Trends Cogn. Sci.* **23**, 213–234 (2019).
8. Matthews, G. A. et al. Dorsal raphe dopamine neurons represent the experience of social isolation. *Cell* **164**, 617–631 (2016).
9. Vander Weele, C. M. et al. Dopamine enhances signal-to-noise ratio in cortical-brainstem encoding of aversive stimuli. *Nature* **563**, 397–401 (2018).

10. Patriarchi, T. et al. Ultrafast neuronal imaging of dopamine dynamics with designed genetically encoded sensors. *Science* **360**, eaat4422 (2018).
11. Sun, F. et al. A genetically encoded fluorescent sensor enables rapid and specific detection of dopamine in flies, fish, and mice. *Cell* **174**, 481–496 (2018).
12. Patriarchi, T. et al. An expanded palette of dopamine sensors for multiplex imaging in vivo. *Nat. Methods* **17**, 1147–1155 (2020).
13. Sun, F. et al. Next-generation GRAB sensors for monitoring dopaminergic activity in vivo. *Nat. Methods* **17**, 1156–1166 (2020).
14. Hamid, A. A., Frank, M. J. & Moore, C. I. Wave-like dopamine dynamics as a mechanism for spatiotemporal credit assignment. *Cell* **184**, 2733–2749 (2021).
15. Lee, S. J. et al. Cell-type-specific asynchronous modulation of PKA by dopamine in learning. *Nature* **590**, 451–456 (2021).
16. Kim, H. R. et al. A unified framework for dopamine signals across timescales. *Cell* **183**, 1600–1616 (2020).
17. Liu, C. et al. An action potential initiation mechanism in distal axons for the control of dopamine release. *Science* **375**, 1378–1385 (2022).
18. Feng, J. et al. Monitoring norepinephrine release in vivo using next-generation GRABNE sensors. Preprint at *bioRxiv* https://doi.org/10.1101/2023.06.22.546075 (2023).
19. Baird, G. S., Zacharias, D. A. & Tsien, R. Y. Circular permutation and receptor insertion within green fluorescent proteins. *Proc. Natl Acad. Sci. USA* **96**, 11241–11246 (1999).
20. Pédelacq, J.-D., Cabantous, S., Tran, T., Terwilliger, T. C. & Waldo, G. S. Engineering and characterization of a superfolder green fluorescent protein. *Nat. Biotechnol.* **24**, 79–88 (2006).
21. Zhao, Y. et al. An expanded palette of genetically encoded Ca^{2+} indicators. *Science* **333**, 1888–1891 (2011).
22. Dana, H. et al. Sensitive red protein calcium indicators for imaging neural activity. *eLife* **5**, e12727 (2016).
23. Bindels, D. S. et al. mScarlet: a bright monomeric red fluorescent protein for cellular imaging. *Nat. Methods* **14**, 53–56 (2017).
24. Feng, S. et al. Improved split fluorescent proteins for endogenous protein labeling. *Nat. Commun.* **8**, 370 (2017).
25. Chien, E. Y. T. et al. Structure of the human dopamine D3 receptor in complex with a D2/D3 selective antagonist. *Science* **330**, 1091–1095 (2010).
26. Yin, J. et al. Structure of a D2 dopamine receptor–G-protein complex in a lipid membrane. *Nature* **584**, 125–129 (2020).
27. Sun, B. et al. Crystal structure of dopamine D1 receptor in complex with G protein and a non-catechol agonist. *Nat. Commun.* **12**, 3305 (2021).
28. Zhuang, Y. et al. Structural insights into the human D1 and D2 dopamine receptor signaling complexes. *Cell* **184**, 931–942 (2021).
29. Wu, J. et al. Improved orange and red Ca^{2+} indicators and photophysical considerations for optogenetic applications. *ACS Chem. Neurosci.* **4**, 963–972 (2013).
30. Wan, Q. et al. Mini G protein probes for active G protein-coupled receptors (GPCRs) in live cells. *J. Biol. Chem.* **293**, 7466–7473 (2018).
31. Kroeze, W. K. et al. PRESTO-Tango as an open-source resource for interrogation of the druggable human GPCRome. *Nat. Struct. Mol. Biol.* **22**, 362–369 (2015).
32. Li, S. et al. Multiregional profiling of the brain transmembrane proteome uncovers novel regulators of depression. *Sci. Adv.* **7**, eabf0634 (2021).
33. Klapoetke, N. C. et al. Independent optical excitation of distinct neural populations. *Nat. Methods* **11**, 338–346 (2014).
34. Nagel, G. et al. Channelrhodopsin-2, a directly light-gated cation-selective membrane channel. *Proc. Natl Acad. Sci. USA* **100**, 13940–13945 (2003).
35. Beyer, C. E., Boikess, S., Luo, B. & Dawson, L. A. Comparison of the effects of antidepressants on norepinephrine and serotonin concentrations in the rat frontal cortex: an in-vivo microdialysis study. *J. Psychopharmacol.* **16**, 297–304 (2002).
36. Greengard, P. The neurobiology of slow synaptic transmission. *Science* **294**, 1024–1030 (2001).
37. Chen, Y. et al. Endogenous Gαq-coupled neuromodulator receptors activate protein kinase A. *Neuron* **96**, 1070–1083 (2017).
38. Wang, L. et al. A high-performance genetically encoded fluorescent indicator for in vivo cAMP imaging. *Nat. Commun.* **13**, 5363 (2022).
39. Ney, L. J. et al. Dopamine, endocannabinoids and their interaction in fear extinction and negative affect in PTSD. *Prog. Neuropsychopharmacol. Biol. Psychiatry* **105**, 110118 (2021).
40. Dong, A. et al. A fluorescent sensor for spatiotemporally resolved imaging of endocannabinoid dynamics in vivo. *Nat. Biotechnol.* **40**, 787–798 (2021).
41. Schultz, W., Dayan, P. & Montague, P. R. A neural substrate of prediction and reward. *Science* **275**, 1593–1599 (1997).
42. Hasselmo, M. E. The role of acetylcholine in learning and memory. *Curr. Opin. Neurobiol.* **16**, 710–715 (2006).
43. Jing, M. et al. An optimized acetylcholine sensor for monitoring in vivo cholinergic activity. *Nat. Methods* **17**, 1139–1146 (2020).
44. Howe, M. W. & Dombeck, D. A. Rapid signalling in distinct dopaminergic axons during locomotion and reward. *Nature* **535**, 505–510 (2016).
45. Calipari, E. S. et al. In vivo imaging identifies temporal signature of D1 and D2 medium spiny neurons in cocaine reward. *Proc. Natl Acad. Sci. USA* **113**, 2726–2731 (2016).
46. Popescu, A. T., Zhou, M. R. & Poo, M. Phasic dopamine release in the medial prefrontal cortex enhances stimulus discrimination. *Proc. Natl Acad. Sci. USA* **113**, E3169–E3176 (2016).

Methods

Animals

All procedures for animal surgery and experimentation were performed in accordance with and approved by the laboratory animal care and use committees of Peking University, the Institutional Animal Care and Use Committee at Oregon Health & Science University, the National Institutes of Health Guide for the Care and Use of Laboratory Animals and Harvard Animal Care and Use Committee. Both male and female postnatal day 0 (P0) Sprague-Dawley rats were used to prepare cultured cortical neurons; P48–P90 wild-type C57BL/6N mice (Beijing Vital River Laboratory), wild-type C57BL/6J mice (Beijing Vital River Laboratory), TH-Cre mice (The Jackson Laboratory; B6.Cg-*7630403G23Rik*$^{Tg(Th\text{-}cre)1Tmd}$/J), DAT-Cre mice (The Jackson Laboratory; B6.SJL-*Slc6a3*$^{tm1.1(cre)Bkmn}$/J) and Long Evans rats (Charles River) were used in this study. All animals were housed at 18–23 °C in 40–60% humidity under a normal 12-h light–dark cycle with food and water available ad libitum.

AAV expression

AAV2/9-hSyn-gDA3m (2.8×10^{13} viral genomes (vg) per ml), AAV2/9-hSyn-gDA3h (8.43×10^{13} vg ml^{-1}), AAV2/9-hSyn-gDA3mut (6.21×10^{13} vg ml^{-1}), AAV2/9-hSyn-gDA2m (5.72×10^{13} vg ml^{-1}), AAV2/9-hSyn-dLight1.3b (6.49×10^{13} vg ml^{-1}), AAV2/9-DIO-hSyn-gDA3m (6.2×10^{13} vg ml^{-1}), AAV2/9-EGFP-CAAX (3.5×10^{13} vg ml^{-1}), AAV2/9-hSyn-ACh3.0 (8.0×10^{13} vg ml^{-1}), AAV2/9-hSyn-eCB2.0 (9.2×10^{13} vg ml^{-1}), AAV2/9-hSyn-G-Flamp1 (7.29×10^{13} vg ml^{-1}) and AAV2/9-hSyn-NE2m (1.39×10^{13} vg ml^{-1}) were packaged at Vigene Biosciences. AAV2/9-hSyn-rDA1m (1.04×10^{13} vg ml^{-1}), AAV2/9-hSyn-rDA2m (6.04×10^{12} vg ml^{-1}), AAV2/9-hSyn-rDA2h (5.31×10^{12} vg ml^{-1}), AAV2/9-hSyn-rDA2mut (5.09×10^{12} vg ml^{-1}), AAV2/9-hSyn-rDA3m (3.29×10^{12} vg ml^{-1}), AAV2/9-hSyn-rDA3h (6.36×10^{12} vg ml^{-1}), AAV2/9-hSyn-rDA3mut (6.16×10^{12} vg ml^{-1}), AAV2/9-hSyn-RdLight1 (6.12×10^{12} vg ml^{-1}), AAV2/9-hSyn-hChR2(H134R)-eYFP (5.49×10^{12} vg ml^{-1}) and AAV2/9-hSyn-ChrimsonR-tdTomato (2.52×10^{12} vg ml^{-1}) were packaged at BrainVTA. AAV9-hSyn-eGFP ($\geq 7 \times 10^{12}$ vg ml^{-1}) was obtained from Addgene (no. 50465). Where indicated, the AAVs were either used to infect cultured neurons or were injected in vivo into specific brain regions.

Molecular biology

Complementary DNAs encoding the various DA receptors were cloned from the respective human (hORFeome database 8.1, http://horfdb.dfci.harvard.edu/index.php?page=home), bovine, sheep, water-bear, bat, cat, monkey, zebrafinch and red fire ant genes (Shanghai Generay Biotech). Plasmids were generated using Gibson assembly[47], and all plasmid sequences were verified using Sanger sequencing. For screening and characterization in HEK293T cells, the green and red fluorescent DA sensors were cloned into the pDisplay vector (Invitrogen). The IRES-mCherry-CAAX cassette (for expressing green fluorescent sensors) or IRES-EGFP-CAAX cassette (for expressing red fluorescent sensors) was inserted downstream of the sensor gene to serve as a cell membrane marker and to calibrate the sensor's fluorescence. Site-directed mutagenesis was performed using primers containing randomized NNB codons (48–51 codons in total, encoding all 20 amino acids; Tsingke Biological Technology) or defined codons. For characterization in cultured neurons, the sensor gene was cloned into a pAAV vector under the control of the human synapsin (*SYN1*) promoter (*pAAV-hSyn*). For luciferase complementation assay, the receptor-SmBit or sensor-SmBit was generated from β_2AR-SmBit (ref. 30). For the Tango assay, genes encoding the wild-type receptors or the indicated sensors were cloned into the pTango vector[31].

Cell culture

HEK293T cells were cultured at 37 °C in humidified air containing 5% CO_2 in DMEM (Biological Industries) supplemented with 10% (vol/vol) FBS (Gibco) and 1% penicillin-streptomycin (Gibco). Rat cortical neurons were prepared from P0 Sprague-Dawley rats. In brief, cortical neurons were dissociated from the dissected rat cerebral cortex by digestion in 0.25% trypsin-EDTA (Biological Industries) and then plated on poly-D-lysine-coated (Sigma-Aldrich) 12-mm glass coverslips in 24-well plates. The neurons were cultured in Neurobasal medium (Gibco) containing 2% B-27 supplement (Gibco), 1% GlutaMAX (Gibco) and 1% penicillin-streptomycin (Gibco) at 37 °C in humidified air containing 5% CO_2. The cultured neurons were transfected with AAVs expressing the indicated sensors at 3–5 d in vitro (DIV3–5) and imaged at DIV11–14.

Fluorescence imaging of cultured cells

Before imaging, the culture medium was replaced with Tyrode's solutions containing (in mM): 150 NaCl, 4 KCl, 2 $MgCl_2$, 10 HEPES and 10 glucose (pH adjusted to 7.35–7.45 with NaOH). The cells then were imaged in a custom-made chamber using an inverted Ti-E A1 confocal microscope (Nikon) with the NIS-Element 4.51.00 software (Nikon) and an Opera Phenix high-content screening system (PerkinElmer) with the Harmony 4.9 software (PerkinElmer). The confocal microscope was equipped with a ×10/0.45-numerical aperture (NA) objective, a ×20/0.75-NA objective, a ×40/1.35-NA oil-immersion objective, a 488-nm laser and a 561-nm laser. Green fluorescence was collected using a 525/50-nm filter, and red fluorescence was collected using a 595/50-nm filter. During imaging, the following compounds were applied via bath application or via a custom-made perfusion system at the indicated concentrations: DA (Sigma-Aldrich), SCH (Tocris), eticlopride (Tocris), SKF-81297 (Tocris), quinpirole (Tocris), glutamate (Sigma-Aldrich), GABA (γ-aminobutyric acid) (Tocris), levodopa (Abcam), ACh (Solarbio), serotonin (Tocris), histamine (Tocris), octopamine (Tocris), NE (Tocris) and sulpiride (MedChemExpress). $\Delta F/F_0 = (F - F_0)/F_0$ was computed by defining F_0 (the baseline fluorescence) as the average fluorescence measured 0–1 min before drug application. To measure the kinetics of the $GRAB_{DA}$ sensors, the confocal line-scanning mode (2,600 Hz) was used to record the fluorescence response when the cells were locally puffed with DA via a pipette positioned at the cells. Similarly, the decay kinetics were measured by locally puffing cells with the respective antagonist in the presence of saturating DA concentration. The Opera Phenix system was equipped with a ×20/1.0-NA objective, a ×40/0.6-NA objective, a ×40/1.15-NA water-immersion objective, a 488-nm laser and a 561-nm laser. Green fluorescence was collected using a 525/50-nm emission filter, and red fluorescence was collected using a 600/30-nm emission filter, and the fluorescence intensity of the red and green fluorescent sensors was calibrated using EGFP and mCherry, respectively.

Spectra and photoactivation measurements

Plasmids expressing the $GRAB_{DA}$ sensors were transfected into HEK293T cells in six-well plates (for one-photon spectra) or on 12-mm coverslips (for two-photon spectra). For measuring the one-photon spectra, the cells were collected 24–30 h after transfection and transferred to 384-well plates in the absence or presence of 100 μM DA. The excitation and emission spectra were then measured at 5-nm increments using a Safire2 multi-mode plate reader (Tecan). The fluorescence measured in nontransfected cells was subtracted as background. The two-photon spectra of gDA3m were measured at 10-nm increments ranging from 700 to 1,050 nm using an Ultima Investigator two-photon microscope (Bruker) equipped with a ×20/1.00-NA water-immersion objective (Olympus), an InSight X3 tunable laser (Spectra-Physics) and the Prairie View 5.5 software (Bruker). The two-photon spectra of rDA3m were measured at 10-nm increments ranging from 820 to 1,300 nm using an A1R MP+ multiphoton microscope (Nikon) equipped with a ×25/1.10-NA objective (Nikon) and a Chameleon Discovery tunable laser (Coherent). Laser power was calibrated according to the output power of the tunable two-photon laser with various wavelengths.

Bursts of 488-nm laser light (1-s duration, 210 µW, ~0.4-W cm^{-2} intensity) were applied to induce blue-light-mediated photoactivation.

Luciferase complementation assay

At 50–60% confluence, HEK293T cells were cotransfected with the indicated wild-type receptor or sensor together with the respective LgBit-mG construct. Approximately 24–36 h after transfection, the cells were dissociated using a cell scraper, resuspended in PBS and transferred to 96-well plates. DA at concentrations ranging from 0.01 nM to 100 µM and 5 µM furimazine (NanoLuc Luciferase Assay, Promega) were then bath-applied to the cells. After a 10-min reaction in the dark at room temperature, luminescence was measured using a VICTOR X5 multi-label plate reader (PerkinElmer).

Tango assay

The Tango assay was performed using HTLA cells (a gift from Bryan L. Roth) seeded in six-well plates and transfected with plasmids expressing the indicated receptors or sensors. At 24 h after transfection, the cells were collected using trypsin digestion and plated in 96-well plates, and DA was added to the media at concentrations ranging from 0.01 nM to 10 µM. The cells were then cultured for an additional 12 h for luciferase expression; 5 µM Bright-Glo (Fluc Luciferase Assay System, Promega) was then added to the wells, and luminescence was measured using a VICTOR X5 multi-label plate reader (PerkinElmer).

Two-photon imaging in the NAc in acute mouse brain slices

Adult (6–8 weeks of age) C57BL/6N mice of both sexes were anesthetized with an intraperitoneal injection of 2,2,2-tribromoethanol (Avertin, 500 mg per kg of body weight; Sigma-Aldrich), and AAVs were injected (300 nl per injection site at a rate of 40 nl min^{-1}) into the NAc using the following coordinates: anterior-posterior (AP): +1.4 mm relative to bregma; medial-lateral (ML): ±1.2 mm relative to bregma; and dorsal-ventral (DV): −4.0 mm from the dura. At 2 weeks after virus injection, the mice were deeply anesthetized, and the heart was perfused with slicing buffer containing (in mM): 110 choline chloride, 2.5 KCl, 1.25 NaH_2PO_4, 25 $NaHCO_3$, 7 $MgCl_2$, 25 glucose and 0.5 $CaCl_2$. The mice were then decapitated and the brains were immediately removed and placed in cold oxygenated slicing buffer. The brains were sectioned into 300-µm-thick coronal slices using a VT1200 vibratome (Leica), and the slices were incubated at 34 °C for at least 40 min in oxygenated artificial cerebrospinal fluid containing (in mM): 125 NaCl, 2.5 KCl, 1 NaH_2PO_4, 25 $NaHCO_3$, 1.3 $MgCl_2$, 25 glucose and 2 $CaCl_2$. Two-photon imaging was performed using either an FV1000MPE two-photon microscope (Olympus) equipped with a ×25/1.05-NA water-immersion objective and a mode-locked Mai Tai Ti:Sapphire laser (Spectra-Physics) and the FV10-ASW v.3.1a software (Olympus) or an Ultima Investigator two-photon microscope (Bruker) equipped with a ×20/1.00-NA objective (Olympus) and an InSight X3 tunable laser (Spectra-Physics) and the Prairie View 5.5 software (Bruker). A 920-nm laser was used to excite the gDA3m sensor, and fluorescence was collected using a 495–540-nm filter (for the FV1000MPE microscope) or a 490–560-nm filter (for the Ultima Investigator microscope); a 950-nm laser was used to excite the rDA3m sensor, and fluorescence was collected using a 575–630-nm filter (for the FV1000MPE microscope) or a 570–620-nm filter (for the Ultima Investigator microscope). For electrical stimulation, a bipolar electrode (model WE30031.0A3, MicroProbes) was positioned near the NAc core under fluorescence guidance, and imaging and stimulation were synchronized using an Arduino board with custom-written software. The stimulation voltage was set at 4–6 V. Where indicated, compounds were added by perfusion at a flow rate of 4 ml min^{-1}.

Two-photon imaging in the striatum and SNc in acute mouse brain slices

Adult TH-Cre and wild-type mice of both sexes were anesthetized with isoflurane, and the indicated AAVs were injected into the SNc region at the following coordinates: AP: −2.3 mm relative to bregma; ML: ±1.3 mm relative to bregma; and DV: −4.5 mm from the dura. After 2–3 weeks, the mice were anesthetized with isoflurane and decapitated, and the brain was removed and placed in warm (32–35 °C) extracellular solution containing (in mM): 126 NaCl, 2.5 KCl, 1.2 $MgCl_2$, 2.4 $CaCl_2$, 1.4 NaH_2PO_4, 25 $NaHCO_3$ and 11 dextrose; the solution also contained MK-801 (10 µM) to prevent NMDA-mediated excitotoxic damage. Horizontal slices (222-µm thickness) containing the midbrain and striatum were cut using a vibratome in warm extracellular solution and recovered at 30 °C for ≥30 min before experiments. Two-photon imaging of the striatal and SNc slices was performed using a custom-built two-photon microscope with ScanImage 3.8.1 software[48]. Full-frame images (128 × 128 pixels) were captured at a rate of 4 Hz. Line scans through areas of interest were taken at 2 ms per line. Images were analyzed using ImageJ (National Institutes of Health) and custom software written using MATLAB.

In vivo fiber photometry recording in mice

Adult mice were anesthetized with isoflurane, and the indicated AAVs (300-nl total volume) were injected as follows. The NAc was targeted using the following coordinates: AP: +1.4 mm relative to bregma; ML: ±1.2 mm relative to bregma; and DV: −4.0 mm from the dura. The mPFC was targeted using the following coordinates: AP: +1.98 mm relative to bregma; ML: ±0.3 mm relative to bregma; and DV: −1.8 from the dura. Finally, the BLA was targeted using the following coordinates: AP: −1.4 mm relative to bregma; ML: ±3 mm relative to bregma; and DV: −4.5 mm from the dura. Optical fibers (200-µm diameter, 0.37 NA; Inper) were implanted using the AAV injection site and secured with resin cement (3M). At 2 weeks after injections, photometry and animal behaviors were recorded using an FPS-410/470/561 photometry system (Inper) with the Inper signal v.2.0.0 software (Inper). In brief, a 10-Hz (with 20-ms pulse duration) 470/5-nm filtered light-emitting diode (LED) at 20–30 µW was used to excite the green fluorescent sensors, and a 10-Hz (20-ms pulse duration) 561/5-nm filtered LED at 20–30 µW was used to excite the red fluorescent sensors. Alternating excitation wavelengths were delivered, and the fluorescence signals were collected using a CMOS camera during dual-color imaging. To minimize autofluorescence of the optical fiber, the recording fiber was photobleached using a high-power LED before recording. The photometry data were analyzed using a custom-written MATLAB (MATLAB R2022a, MathWorks) program, and background autofluorescence was subtracted from the recorded signals.

Unpredicted water reward. Adult female (8–9 weeks in age) C57BL/6J mice were prepared for this experiment. AAV-hsyn-rDA3m or AAV-hsyn-RdLight1 virus (300 nl for each virus) was bilaterally injected into the NAc. Intraoral cheek fistula-implanted and water-restricted mice freely received water delivery (around 10 µl per trial; 25 trials per session; interreward interval = 20 s). To calculate $\Delta F/F_0$, baseline was chosen as the average fluorescence signal during 4.5–5.0 s ahead of water delivery.

Mating behaviors. Adult (8–9 weeks of age) male C57BL/6N mice were used for these experiments. A mixture of AAV-hsyn-rDA3m (300 nl) and AAV-hsyn-G-Flamp1 (300 nl) was injected into the NAc as described above. Experienced adult (8–9 weeks in age) ovariectomized female C57BL/6N mice were also used to measure the male's mating behaviors. At 3 d before recording, the ovariectomized female mice received intraperitoneal injections of estrogen (50 µl, 0.2 mg ml^{-1} on day 1; and 50 µl, 0.1 mg ml^{-1} on day 2) or progesterone (50 µl, 1 mg ml^{-1} on day 3). To calculate $\Delta F/F_0$, the baseline was defined as the average fluorescence measured 1–5 min before introducing the female.

Foot shock. Adult (8–9 weeks of age) male C57BL/6N mice were used for these experiments. A mixture of AAV-hsyn-eCB2.0 (300 nl) and either AAV-hsyn-rDA2m or AAV-hsyn-rDA1m (300 nl each) was

bilaterally injected into the BLA as described above. The mouse was placed in a shock box, and five 2-s pulses of electricity at an intensity of 0.7 mA were delivered with an interval of 90–120 s between trials. To calculate $\Delta F/F_0$, the baseline value was defined as the average fluorescence measured during a 2-s window before the first shock trial.

Pavlovian auditory conditioning task. Adult (8–9 weeks of age) female C57BL/6J mice were used for these experiments. A mixture of AAV-hsyn-gACh3.0 (300 nl) and AAV-hsyn-rDA3m (300 nl) was injected into the NAc and mPFC as described above. A stainless-steel head holder was attached to the skull using resin cement to restrain head-fix the animal. For water delivery, an intraoral cheek fistula was implanted in each mouse. In brief, incisions were made in the cheek and the scalp at the back of the neck. A short, soft silastic tube (inner diameter: 0.3 mm; outer diameter: 0.46 mm) connected via an L-shaped stainless-steel tube was then inserted into the cheek incision site. The steel tube was inserted into the scalp incision, and the opposite end was inserted into the oral cavity. The head-fixed mice were habituated to the treadmill apparatus for 2 d (1 h per day) before the experiments to minimize potential stress. On the day of the experiment, the Pavlovian auditory conditioning task was performed using two pairs of auditory cues and outcomes, with tone A (2.5 kHz, 70 dB, 2-s duration) paired with delivery of 10 µl of 5% sucrose water and tone B (15 kHz, 70 dB, 2-s duration) paired with delivery of an air puff to the eye. These two pairs were randomly delivered with a 15–20-s randomized intertrial interval. The water and air puff delivery were precision-controlled using a stepper motor pump and a solenoid valve, respectively. A custom Arduino code was used to control the timing of the pump and solenoid valve and to synchronize the training devices with the photometry recording system. To calculate $\Delta F/F_0$, the baseline was defined as the average fluorescence signals measured 4.5–5.0 s before the first auditory cue.

Fiber photometry recording of optogenetically induced DA release in mice

Adult (8–9 weeks of age) male C57BL/6N mice were used for these experiments. To validate the green DA sensors with optogenetics, mice were anesthetized, and AAV-hsyn-gDA3h or AAV-hsyn-dLight1.3b was injected into the mPFC (AP: +1.98 mm relative to bregma; ML: ±0.3 mm relative to bregma; and DV: −1.8 from the dura), AAV-hsyn-ChrimsonR-tdTomato was injected into the VTA (AP: −2.9 mm relative to bregma; ML: ±0.65 mm relative to bregma; and DV: −4.1 mm from the dura) and optical fibers (200-µm diameter, 0.37 NA; Inper) were implanted in the same injection sites. At 2 weeks after virus injection, photometry recording was performed using a commercially available photometry system (Thinker Tech) with the Multi Channel Fiber Photometry software.

A 470/25-nm bandpass-filtered (model 65–144; Edmund Optics) LED light (Cree LED) was used to excite the green fluorescent sensors. The emitted fluorescence was bandpass filtered (525/25 nm, model 86–354; Edmund Optics) and collected using a photomultiplier tube (model H10721-210; Hamamatsu). An amplifier (model C7319; Hamamatsu) was used to convert the current output from the photomultiplier tube to a voltage signal that was passed through a low-pass filter. The analog voltage signals were then digitized using an acquisition card (National Instruments). To minimize autofluorescence of the optical fiber, the recording fiber was photobleached using a high-power LED before recording. The excitation light power at the tip of the optical fiber was 20–30 µW and was delivered at 100 Hz with 5-ms pulse duration. Background autofluorescence was subtracted from the recorded signals in the subsequent analysis. A 635-nm laser (1–300 mW; LL-Laser) was used for optogenetic stimulation with the light power at the tip of the fiber set at 10 mW. Optical stimulation was delivered at 20 Hz (20-ms pulse duration) for a total of 1–20 pulses simultaneously with photometry recording. Where indicated, the mice received an intraperitoneal injection of SCH (2 mg per kg of body weight).

When validating the red-shifted $GRAB_{DA}$ sensors, AAV-hsyn-rDA3m or AAV-hsyn-rDA3mut was injected into the central amygdala (AP: −1 mm relative to bregma; ML: ±2.5 mm relative to bregma; and DV: −4.3 mm from the dura). In addition, AAV-hsyn-rDA2m or AAV-hsyn-rDA2mut was injected in the mPFC and NAc, AAV-hsyn-ChR2-YFP was injected into the VTA and optical fibers were implanted at the same injection sites. At 2 weeks after injection, photometry recording (FPS-410/470/561; Inper) was performed was described above. A 488-nm laser (1–160 mW, LL-Laser) was used for optogenetic stimulation, with the light power at the tip of the fiber set at 10 mW. Optical stimulation was delivered at 20 Hz (1, 5 or 10 s duration) simultaneously with photometry recording. Where indicated, the mice received an intraperitoneal injection of SCH (6 mg per kg of body weight).

Behavioral assays in rodents

Adult male C57BL/6J mice (8–9 weeks of age) were used for the mouse experiments. Mice were anesthetized, and AAV9-hSyn-gDA3h, AAV9-hSyn-rDA3h and AAV9-hSyn-EGFP-CAAX (or AAV9-hSyn-EGFP) were injected into the NAc bilaterally. The diverse cohort of mice was subjected to open-field test, cocaine-induced hyperlocomotion test and odor–reward associative learning task[49] at least 2 weeks after surgery. Mice were handled for 3 d for 3 min each day before experiments. For cocaine self-administration, adult (>10 weeks at start of experiment) wild-type Long Evans rats from both sexes were used. The behavior assays were blindly analyzed.

Open-field test in mice. The open-field test was performed in ENV-510 test chambers (27.3 × 27.3 × 20.3 cm^3, Med Associates). The chamber is equipped with infrared photo beams, which were used to evaluate spontaneous mouse locomotor activity. At the start of the test, mice were placed in the center of the arena, and were allowed to freely explore the environment for 10 min. Mouse movement was tracked and analyzed by the Activity Monitor 7 software (Med Associates) for the total travel distance, the number of entries to the central zone (14.29 × 14.29 cm^2) and the time spent in the central zone.

Cocaine-induced hyperlocomotion in mice. On each day of the experiment, mice were brought into the testing room for 1 h of habituation. Experiments were performed during the light cycle at a consistent time of day. For day 1, mice received an intraperitoneal injection of 10 µl of sterile saline per gram of body weight and were immediately tested for locomotor activity for 30 min. On the subsequent day, mice received an intraperitoneal injection of 10 mg kg^{-1} cocaine in the same volume of saline. The fold change in locomotion activity was calculated as the total distance in 30 min after receiving cocaine divided by that after receiving saline.

Odor–reward associative learning task in mice. Mice were water-deprived for 48 h and then habituated to the head-fixed setup. Delivery of odor and water and registration of licks were controlled by an Arduino-based system running on MATLAB (MathWorks). Briefly, in associative training sessions, the water reward was preceded by an odor (valve opening for approximately 1 s). The interval between odor onset and water delivery was 3 s. The intertrial interval was randomized between 6 s and 8 s. Mice were trained for approximately 30 reward trials per day. Daily performance was analyzed in MATLAB as previously described.

Cocaine self-administration in rats. Rats had ~7 d to acclimate after arriving before undergoing any experimental procedures. Then, they underwent intracranial surgery to infuse virus (either eGFP or gDA3m) bilaterally into the NAc core. Two injections, 250 nl each, were performed in each hemisphere (AP: +1.3 mm; ML: ±2.4 mm; DV: −7.2 mm for the first injection and −7.0 mm for the second injection; 6° angle). Virus was injected at a rate of 100 nl min^{-1}, and the injector tip was left

in place for 5 min after injection. For this surgery and the other surgery described below, rats were anesthetized using inhalable isoflurane (~5% for induction and then maintained at ~2%), and meloxicam (5 mg kg^{-1}, subcutaneous, Covetrus) was administered during the surgical procedure and for 24 h following completion of the surgery. After 7 d of recovery from virus surgery, rats underwent a second surgery to implant a silastic catheter (PlasticsOne) into the right jugular vein[50,51]. Intravenous catheters were flushed with cefazolin (0.1 ml of 0.1 g ml^{-1} in sterile 0.9% saline) to prevent infection and maintain catheter patency. Following completion of the surgery, rats were monitored until they were awake and active, and were singly-housed for the duration of the experiment. After 6 d of recovery, rats were allowed to self-administer cocaine (0.5 mg kg^{-1} per infusion, 6 h d^{-1}, during the dark cycle) for 10 d on a fixed ratio 1 schedule[50,51]. We used operant chambers (MED Associates) held within sound-attenuating cabinets and equipped with two nose-poke holes. Responding in the active hole resulted in an intravenous infusion of cocaine and the illumination of a cue light within the nose-poke hole. Responding in the inactive hole was recorded but had no consequences. Cocaine HCl was obtained from the National Institute on Drug Abuse and dissolved in 0.9% saline. After completion of self-administration training, 13 rats (8 eGFP and 5 gDA3m) were perfused and virus expression in the NAc was verified. The other three gDA3m rats were killed and brain slices prepared to verify that virus was expressed in the NAc and that electrical stimulation of the NAc resulted in detection of DA release.

Fiber photometry recording of DA signals in mice receiving water rewards

AAVs carrying $GRAB_{DA}$ DA sensors were injected into the NAc of DAT-Cre mice (300 nl, unilateral injection; $gGRAB_{DA2m}$: AAV9-hsyn-gDA2m, titer = 2.3×10^{13} vg ml^{-1}; $gGRAB_{DA3m}$: AAV9-hsyn-gDA3m, titer = 1.3×10^{13} vg ml^{-1}). For red $GRAB_{DA}$ sensors, we injected a mixture of AAVs carrying $rGRAB_{DA}$ and GFP (3:1 mixture, 300-nl total volume; GFP: AAV8-CAG-GFP, titer = 6.7×10^{12} vg ml^{-1}; $rGRAB_{DA1m}$: AAV9-hsyn-rDA1m, titer = 2.5×10^{13} vg ml^{-1}; $rGRAB_{DA3m}$: AAV9-hsyn-rDA3m, titer = 6×10^{12} vg ml^{-1}). NAc coordinates were, from bregma: AP 1.5 mm, ML 1.7 mm, DV 4.0 mm, angled 4° forward. An optical fiber was implanted targeting NAc (400-µm diameter, NA = 0.48, Doric Lenses).

At least 2 weeks after surgery, mice were water-restricted (to 85% of initial body weight) and trained to receive water rewards while head-fixed. After mice consistently licked to water delivery (typically requiring 3 d of training), we recorded DA sensor responses to unpredicted delivery of water droplets of various sizes (1, 2, 4 or 8 µl; interreward interval = 8–20 s, uniformly distributed; 60 trials per session, 15 trials per reward size, randomly interleaved; in some sessions, only 2 or 8 µl of water was given). Photometry signals were collected with a bundle-imaging fiber photometry system (Doric Lenses). For green DA sensors, we used a blue LED (460–490 nm, 75 µW measured at tip of patch cord) to excite the sensor and the isosbestic wavelength as a control signal (410–420-nm LED, 60 µW). For red DA sensors, we used a yellow LED (555–570 nm, 110 µW) to excite the sensor and GFP signals as a control (460–490-nm LED, 75 µW). Imaging was performed at 20 Hz. Photometry data were processed offline as follows. $\Delta F/F_0 = (F - F_0)/F_0$ was computed by defining F_0 as the tenth percentile of each signal within a sliding 30-s window (excluding reward responses, defined as the 5 s following reward). Then, linear regression was performed between the sensor signal and the control signal (either isosbestic wavelength or GFP) in inter-trial intervals (5 s following reward delivery excluded). The resulting predicted signal was subtracted from the sensor signal to produce the final de-noised signal.

Two-photon in vivo imaging in mice

Adult (7–8 weeks of age) female C57BL/6N mice were used for these experiments. The mice were anesthetized with isoflurane (3% induction, followed by 1–1.5% maintenance), the skin and skull above the motor cortex were removed and a metal recording chamber was affixed to the head. AAV expressing gDA3m, gDA3h, dLight1.3b or mEGFP (200 nl each, full titer) was then injected into the motor cortex using the following coordinates: AP: +1.0 mm relative to bregma; ML: ±1.5 mm relative to bregma; and DV: −0.5 mm from the dura). A 4 mm × 4 mm square glass coverslip was then used to cover the opening in the skull. A stainless-steel head holder was attached to the skull to head-fix the animal and reduce motion-induced artifacts during imaging. At 2 weeks after virus injection, the mice were habituated for approximately 10 min on the treadmill imaging apparatus to minimize stress. The motor cortex was imaged at a depth of 100–200 µm below the pial surface using Prairie View 5.5.64.100 software with an Ultima Investigator two-photon microscope (Bruker) equipped with a ×16/0.80-NA water-immersion objective (Olympus) and an InSight X3 tunable laser (Spectra-Physics). A 920-nm laser was used for excitation, and a 525/70-nm emission filter was used to collect the fluorescence signal at a sampling rate of 1.5 Hz. For the forced running paradigm, running speed was set at 15 cm s^{-1}; for the tail shock paradigm, a 3-s electrical shock (0.7 mA) was delivered. For audio stimulation, a 1-s pulse of white noise (80 dB) was delivered. For image analysis, motion-related artifacts were corrected using the EZcalcium motion correction algorithm[52]. Fluorescence intensity measurements at the ROIs were collected using ImageJ software. The fluorescence responses were calculated as $(F_{raw} - F_{baseline})/F_{baseline}$, in which $F_{baseline}$ was defined as the average fluorescence signal measured for 10 s before the behavior onset. The peak response during a behavior was calculated as the maximum $\Delta F/F_0$ measured for 0–5 s after the behavior onset. The brain area was deemed responsive if the average response in a 5-s window surrounding the peak exceeded the sum of the baseline average and the baseline standard deviation. Hierarchical clustering was performed on the average of the fluorescence signals (forced running and shock) for each ROI. Euclidean distance and the Ward linkage metric were used after comparing multiple linkage metrics and clustering algorithms. Variations among individuals were minimized by normalizing the response to the maximum $\Delta F/F_0$ across ROIs in a given mouse. The hierarchical method was used to reduce bias due to predetermining the cluster number.

Immunohistochemistry

Mice were anaesthetized (using Avertin) and intracardially perfused with PBS followed by 4% PFA in PBS buffer, and brains were dissected and fixed at 4 °C overnight by 4% PFA in PBS. Brains were sectioned at 40-µm thickness using a VT1200 vibratome (Leica). Slices were placed in blocking solution containing 5% normal goat serum, 0.1% Triton X-100 and 2 mM $MgCl_2$ in PBS for 1 h at room temperature. Then, slices were incubated in AGT solution (0.5% normal goat serum, 0.1% Triton and 2 mM $MgCl_2$ in PBS) containing primary antibodies, anti-GFP antibody (Abcam, catalog no. ab13970, chicken, dilution 1:1,000) and anti-RFP antibody (Rockland, catalog no. 600-401-379, rabbit, dilution 1:500), overnight at 4 °C. On the following day, slices were rinsed three times in AGT and incubated for 2 h at room temperature with secondary antibodies: Goat anti-Chicken Alexa Fluor 488 (Abcam, catalog no. ab150169, dilution 1:500) and Goat anti-Rabbit iFluor 555 (AAT Bioquest, catalog no. 16690, dilution 1:500). After three washes in AGT, slices were incubated in AGT containing DAPI (MedChemExpress, catalog no. HY-D0814, 5 mg ml^{-1}, dilution 1:1,000) for 15 min at room temperature and then rinsed in PBS. Slices were mounted on slides. Slices were imaged on an Aperio Versa (Leica) under a ×10 objective.

Quantification and statistical analysis

Except where indicated otherwise, all summary data are presented as the mean ± s.e.m. Imaging data were processed using ImageJ (1.53c) or MATLAB software (matlab R2020a and R2022a) and plotted using OriginPro 2020b (OriginLab), GraphPad Prism 8.0.2 or Adobe

Illustrator CC. The SNR was calculated as the peak response divided by the standard deviation of the baseline fluorescence. Group differences were analyzed using a one-way ANOVA with Tukey's multiple comparison test, a one-way ANOVA with Dunnett's multiple comparison test, a two-way ANOVA with Sidak's multiple comparison test, a two-tailed Student's *t*-test or a mixed-effects model (GraphPad Prism 8.0.2). Differences were considered significant at $P < 0.05$; $^{*}P < 0.05$, $^{**}P < 0.01$, $^{***}P < 0.001$, $^{****}P < 0.0001$ and not significant ($P > 0.05$). For all representative images and traces, similar results were obtained for >3 independent experiments.

Reporting summary

Further information on research design is available in the Nature Portfolio Reporting Summary linked to this article.

Data availability

The plasmids and sequences used to express the sensors in this study are available from Addgene (catalog nos. 208692–208708; https://www.addgene.org/Yulong_Li/). Source data are provided with this paper.

Code availability

The custom MATLAB codes, Arduino program and ImageJ programs are available under an MIT license from https://github.com/yulonglilab/FiberPhotometry and https://github.com/yulonglilab/BrainSlices.

References

47. Gibson, D. G. et al. Enzymatic assembly of DNA molecules up to several hundred kilobases. *Nat. Methods* **6**, 343–345 (2009).
48. Pologruto, T. A., Sabatini, B. L. & Svoboda, K. ScanImage: flexible software for operating laser scanning microscopes. *Biomed. Eng. Online* **2**, 13 (2003).
49. Zhu, Y. et al. Dynamic salience processing in paraventricular thalamus gates associative learning. *Science* **362**, 423–429 (2018).
50. Loweth, J. A. et al. Synaptic depression via mGluR1 positive allosteric modulation suppresses cue-induced cocaine craving. *Nat. Neurosci.* **17**, 73–80 (2014).
51. Conrad, K. L. et al. Formation of accumbens GluR2-lacking AMPA receptors mediates incubation of cocaine craving. *Nature* **454**, 118–121 (2008).
52. Cantu, D. A. et al. EZcalcium: open-source toolbox for analysis of calcium imaging data. *Front. Neural Circuits* **14**, 25 (2020).

Acknowledgements

The research was supported by the National Natural Science Foundation of China (grant nos. 31925017) and the NIH BRAIN Initiative (grant nos. 1U01NS113358 and 1U01NS120824); and by grants from the Feng Foundation of Biomedical Research, the Clement and Xinxin Foundation, the New Cornerstone Science Foundation through the New Cornerstone Investigator Program and the XPLORER PRIZE, the Peking-Tsinghua Center for Life Sciences, the State Key Laboratory of Membrane Biology at Peking University School of Life Sciences and the National Key R&D Program of China (2022YFE0108700) to Y.L.; the NIH (grant no. R01DA004523) to J.T.W.; the NIH (grant no. R01MH125162) to M.W.-U.; the NIH (grant no. 5F32MH126505-02) to M.G.C.; the NIH (grant no. R01DA049930) to M.E.W.; the NIH (grant no. F31DA057063) to S.J.W.; the National Key R&D Program of China (grant no. 2022YFC-3300905) to H.D.; and the National Natural Science Foundation of China (grant no. 82171492) to Y. Zhu. We thank I. Green and I. Tsutsui-Kimura for assistance for animal surgery. We thank X. Lei at PKU-CLS and the National Center for Protein Sciences at Peking University in Beijing, China, for support and assistance with the Opera Phenix high-content screening system, imaging platform and behavioral experiments. Cartoon illustrations, including Figs. 1a, 3m, 4a (top), 4g (left), 5a, 6a, 6b, 6c(i), 6d(i), 6e(i), Extended Data Figs. 4, 5, 6, 8a, 8d, and 10, were created with BioRender.com.

Author contributions

Y.L. supervised the study. Y. Zhuo and Y.L. designed the study. Y. Zhuo, X.Y., Y.W., G.L., H.W. and Y. Zheng performed the experiments related to the development, optimization and characterizing of the sensors in cultured HEK293T cells and in neurons. Y. Zhuo., R.C. and T.Q. performed the surgery and two-photon imaging experiments related to the validation of the sensors in acute brain slices. J.T.W. performed the characterization in acute brain slices containing the striatum or SNc. H.D., J.W., B. Li and X.M. performed the in vivo fiber photometry recoding during optogenetic stimulation. M.G.C. performed the fiber photometry recording in the mouse NAc for the independent validation of in vivo sensor comparison under the supervision of M.W.-U. Y. Zhuo and B. Luo performed the in vivo fiber photometry recording in the NAc during mating behavior. B. Luo performed the in vivo fiber photometry recording during foot shock and the Pavlovian conditioning task with help from H.D. Y. Zhuo performed the in vivo two-photon imaging of the motor cortex. L.W. performed immunohistochemistry experiments. Y. Zhuo, B. Luo and F.L. under the supervision of Y. Zhu and S.J.W. under the supervision of M.E.W. performed the behavioral assays. All authors contributed to the interpretation and analysis of the data. Y. Zhuo and Y.L. wrote the manuscript with contributions from all authors.

Competing interests

The authors declare no competing interests.

Additional information

Extended data is available for this paper at https://doi.org/10.1038/s41592-023-02100-w.

Supplementary information The online version contains supplementary material available at https://doi.org/10.1038/s41592-023-02100-w.

Correspondence and requests for materials should be addressed to Yulong Li.

Peer review information *Nature Methods* thanks David Sulzer and the other, anonymous, reviewer(s) for their contribution to the peer review of this work. Primary Handling Editor: Nina Vogt, in collaboration with the *Nature Methods* team.

https://doi.org/10.1038/s41592-023-02100-w

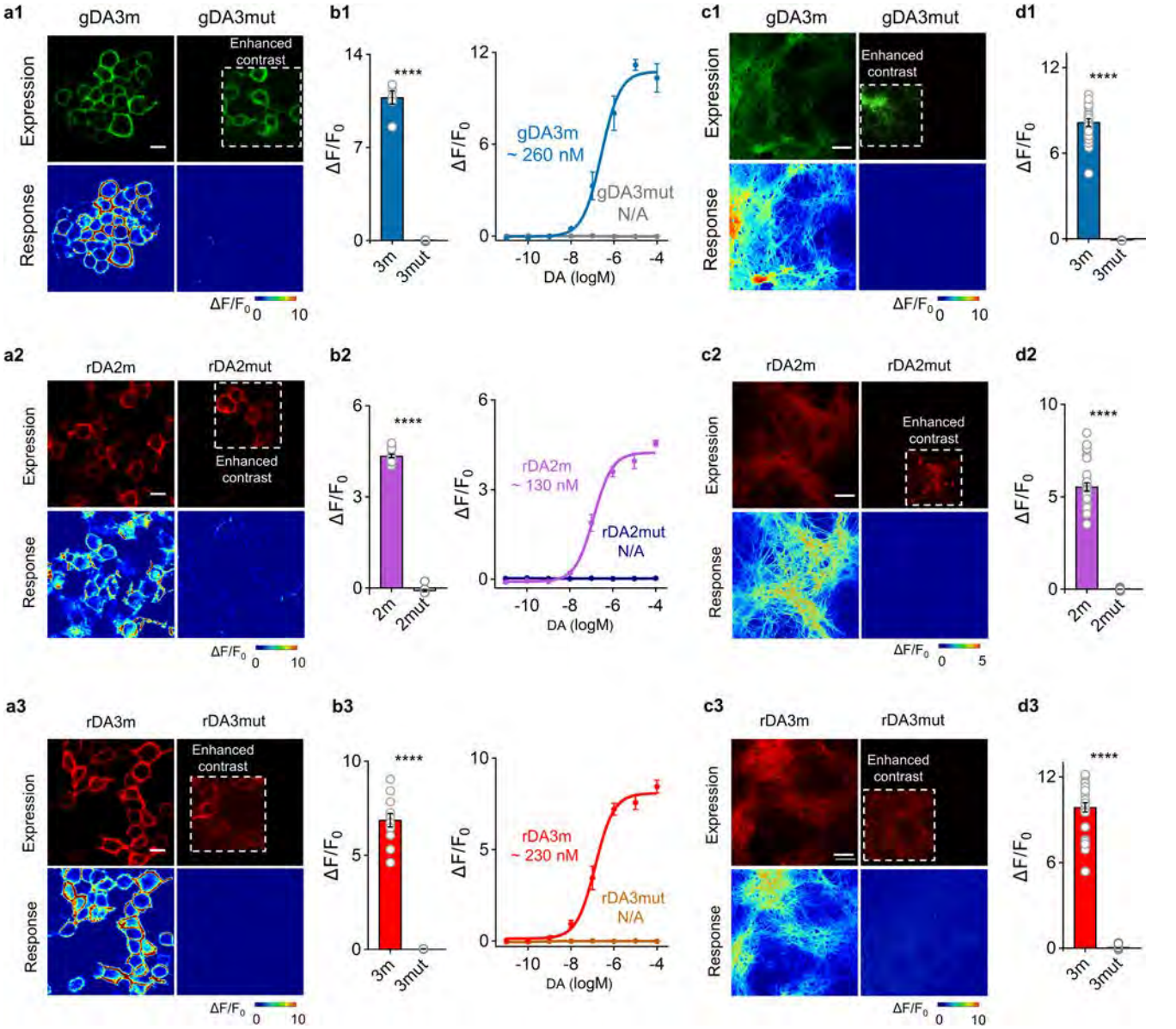

Extended Data Fig. 1 | Performance of DA-insensitive mutant sensors. **a**, Representative images showing sensor expression (top) in HEK293T cells and fluorescence response to 100 μM DA (bottom) of indicated sensor variants. Scale bar, 20 μm. **b**, Group summary of maximal $\Delta F/F_0$ in response to 100 μM DA (left) and titration DA curves (right) of indicated sensors in HEK293T cells. Left, $n = 6$, 6, 15, 15, 12, 3 wells for gDA3m, gDA3mut, rDA2m, rDA2mut, rDA3m and rDA3mut. Each well contains 400–500 cells. Two-tailed Student's t-test was performed. Right, $n = 3$ wells (with 400–500 cells per well) for each group. **c**, Representative images showing sensor expression (top) in cultured neurons and fluorescence response to 100 μM DA (bottom) of indicated sensor variants. Scale bar, 50 μm. **d**, Group summary of maximal $\Delta F/F_0$ of indicated sensors in response to 100 μM DA in cultured neurons. $n = 60$ neurons from 4 cultures for rDA2mut, n = 30/2 for others, mean±s.e.m. Two-tailed Student's t-test was performed.

https://doi.org/10.1038/s41592-023-02100-w

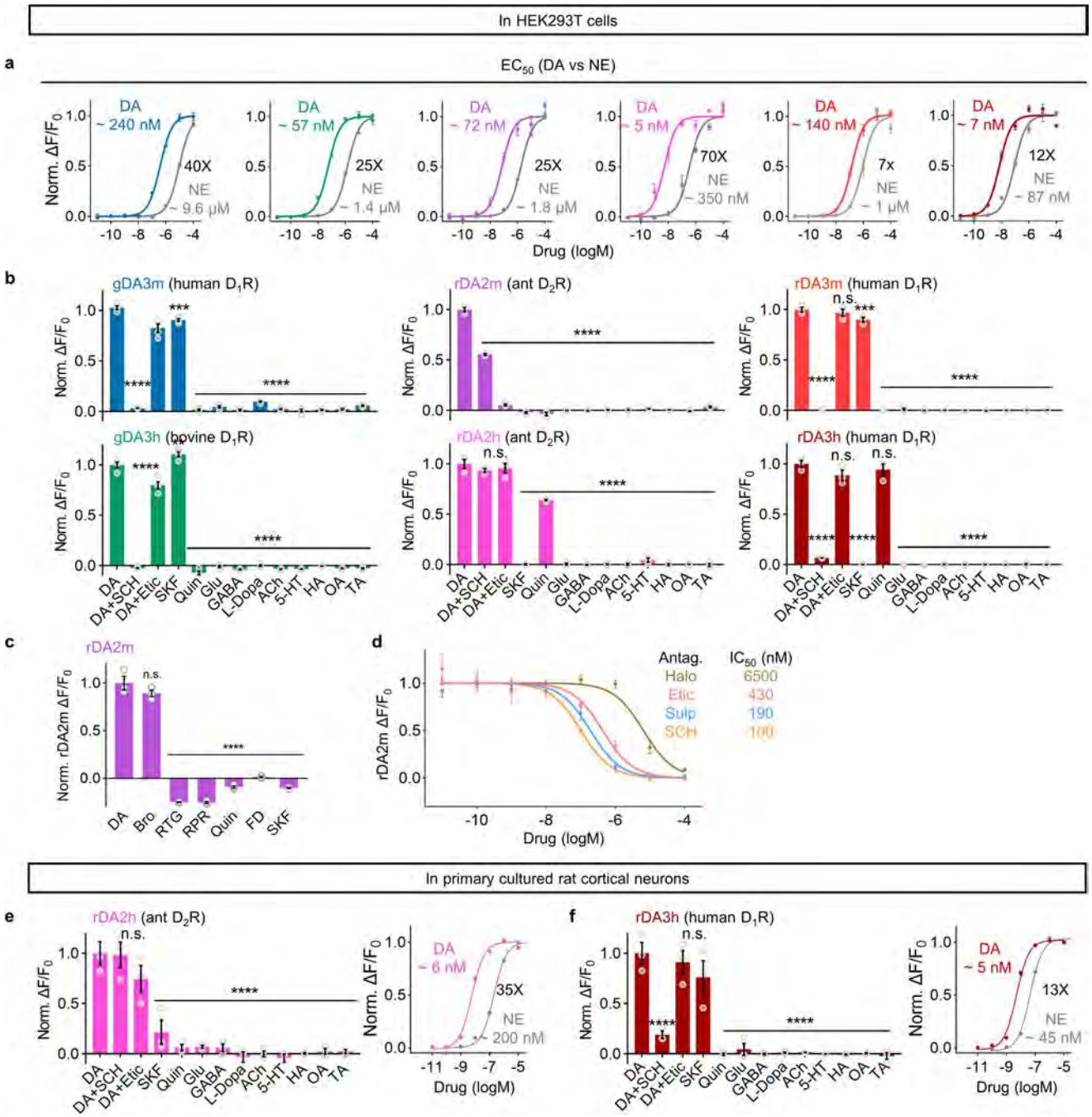

Extended Data Fig. 2 | Pharmacological profiles of GRAB$_{DA}$ sensors measured in cultured cells. a, Titration curves of indicated sensors for the response to DA or NE in HEK293T cells. $n = 3$ cells with 400–500 cells per well, mean±s.e.m. **b**, The normalized $\Delta F/F_0$ in sensor-expressing HEK293T cells in response to the indicated compounds. Antagonists were applied at 10 μM, others at 1 μM. $n = 4$ wells for gDA3m and gDA3h, $n = 3$ wells for others, mean±s.e.m. One-way Anova, post hoc Dunnett's test: gDA3m, $p = 0.0002$, 8.9×10^{-10} between DA and SFK, or DA+Etic, $p = 1.3 \times 10^{-13}$ between DA and others; gDA3h, $p = 0.0020$, 4.3×10^{-9} between DA and SFK, or DA+Etic, $p = 1.3 \times 10^{-13}$ between DA and others; rDA2m, $p = 3.3 \times 10^{-14}$ between DA and others; rDA2h, $p = 0.6059$, 0.9530 between DA and DA + SCH, or DA+Etic, $p = 3.3 \times 10^{-14}$ between DA and others; rDA3m, $p = 0.9182$, 0010 between DA and DA+Etic, or SKF, $p = 3.3 \times 10^{-14}$ between DA and others; rDA3h, $p = 0.0724$, 0.8723 between DA and DA+Etic, or Quin, $p = 3.3 \times 10^{-14}$ between DA and others. **c**, The normalized $\Delta F/F_0$ in rDA2m-expressing HEK293T cells in response to indicated DA agonists. Bromocriptine (Bro), Rotigotine (RTG), D_2R/D_1R agonists; Ropinirole (RPR), Quin, D_2R-specific agonists; Fenodopam (FD), SKF, D_1R-specific agonist. All chemicals were bath-applied in 100 μM. $n = 3$ wells, mean±s.e.m. One-way Anova, post hoc Dunnett's: $p = 0.1074$ between DA and Bro, $p = 8.0 \times 10^{-12}$ between DA and others. **d**, Titration curves of indicated dopamine receptor antagonists. The fluorescence intensity in the presence with 10 μM DA was set as F_0 and the relative fluorescence changes under indicated compound concentration were plotted. $n = 3$ wells with 400–500 cells per well, mean±s.e.m. **e**, **f**, Pharmacological specificity (left) and titration curves of indicated sensors for the response to DA or NE (right) in cultured neurons. Left, antagonists at 10 μM, others at 1 μM. $n = 3$ wells, mean±s.e.m. One-way Anova, post hoc Dunnett's test: rDA2h, $p = 0.9998$, 0.1458 between DA and DA + SCH, or DA+Etic, $p = 1.5 \times 10^{-7}$ between DA and others; rDA3h, $p = 0.9591$, 0.1309 between DA and DA+Etic, or SKF, $p = 4.0 \times 10^{-9}$ between DA and others.

https://doi.org/10.1038/s41592-023-02100-w

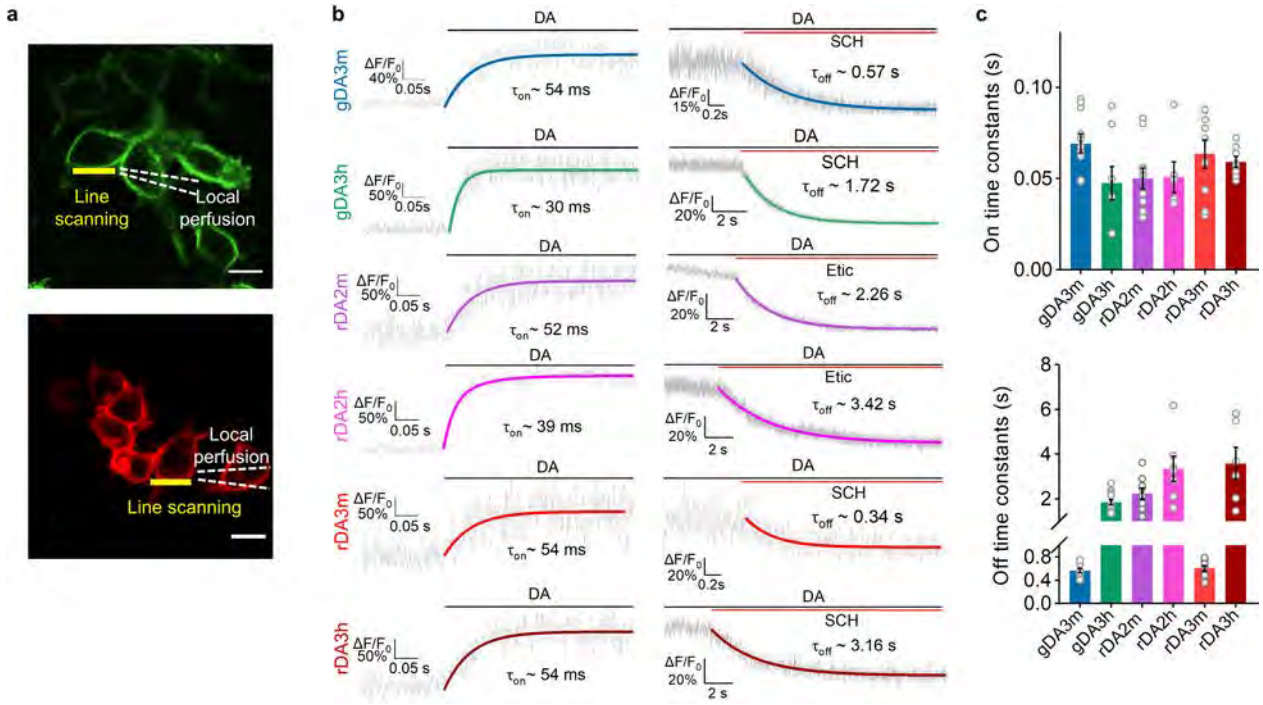

Extended Data Fig. 3 | Kinetics measurement of GRAB$_{DA}$ sensors in HEK293T cells. a, Schematic illustration showing the local perfusion system using a glass pipette containing 100 μM DA and/or receptor-specific antagonist positioned above the sensor-expressing cell. The yellow line indicates the area for line scanning. The dash lines indicate the pipette. Scale bar, 20 μm. **b**, Representative traces showing the response measured using line-scanning; when indicated, DA and receptor-specific antagonist were puffed onto the cell. The trace were the average of 3 different ROIs on the scanning line. Data are shown as mean ± SD. Each trace was fitted with a single-exponential function to determine the τ_{on} (left) and τ_{off} (right). **c**, Group summary of τ_{on} and τ_{off}. τ_{on}, n = 11, 8, 11, 6, 9, 8 cells for gDA3m, gDA3h, rDA2m, rDA2h, rDA3m, rDA3h; τ_{off}, n = 10, 14, 9, 7, 10, 6 cells for gDA3m, gDA3h, rDA2m, rDA2h, rDA3m, rDA3h, mean±s.e.m.

https://doi.org/10.1038/s41592-023-02100-w

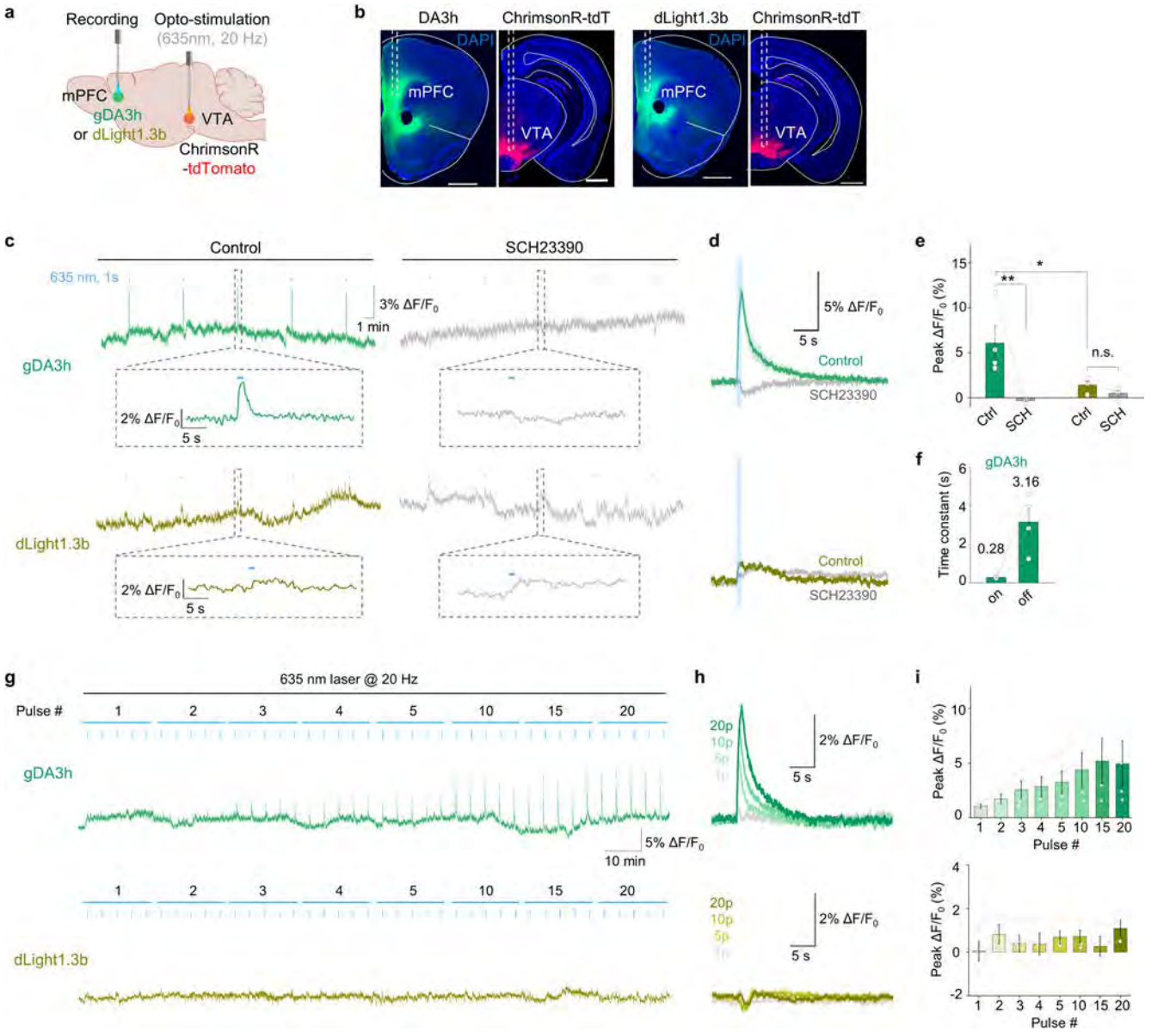

Extended Data Fig. 4 | gGRAB$_{DA3h}$ sensors report optogenetically-elicited DA release in the mouse mPFC. a, Schematic illustration depicting the experimental design for panel **b**-**i**. **b**, Histological verification of indicated sensor expression in mPFC and ChrimsonR expression in VTA. Dashed boxes indicate the location of optical tract. Scale bar, 1 mm. **c**, Representative fluorescence changes and zoom-in view (indicated by dashed box) of indicated sensors during optogenetic stimulations under control condition or in the presence of SCH-23390 (SCH). **d**, Average traces of the change in gDA3h (top) or dLight1.3b (bottom) fluorescence from a mouse. Data are shown as mean±s.d. **e**, Group summary of $\Delta F/F_0$ for the indicated sensors. $n = 4$ mice for gDA3h and dLight1.3b, respectively, mean±s.e.m. One-way ANOVA, post hoc Tukey's test was performed. **p = 0.0035 for gDA3h; n.s. p = 0.9122 for dLight1.3b; *p = 0.0295 between gDA3h and dLight1.3b. **f**, Group summary of the rise and decay time constant of the gDA3h signals in response to optogenetic stimulations. $n = 4$ mice, mean±s.e.m. **g**, **h**, Example fluorescence response (**g**) and corresponding average traces (**e**) of gDA3h (top) or dLight1.3b (bottom) to indicated optogenetic stimulation. The average traces are shown as mean±s.d. **i**, Group summary of peak $\Delta F/F_0$ of gDA3h or dLight1.3b in response to indicated optogenetic stimulation. $n = 4$ mice for gDA3h and dLight1.3b, mean±s.e.m.

https://doi.org/10.1038/s41592-023-02100-w

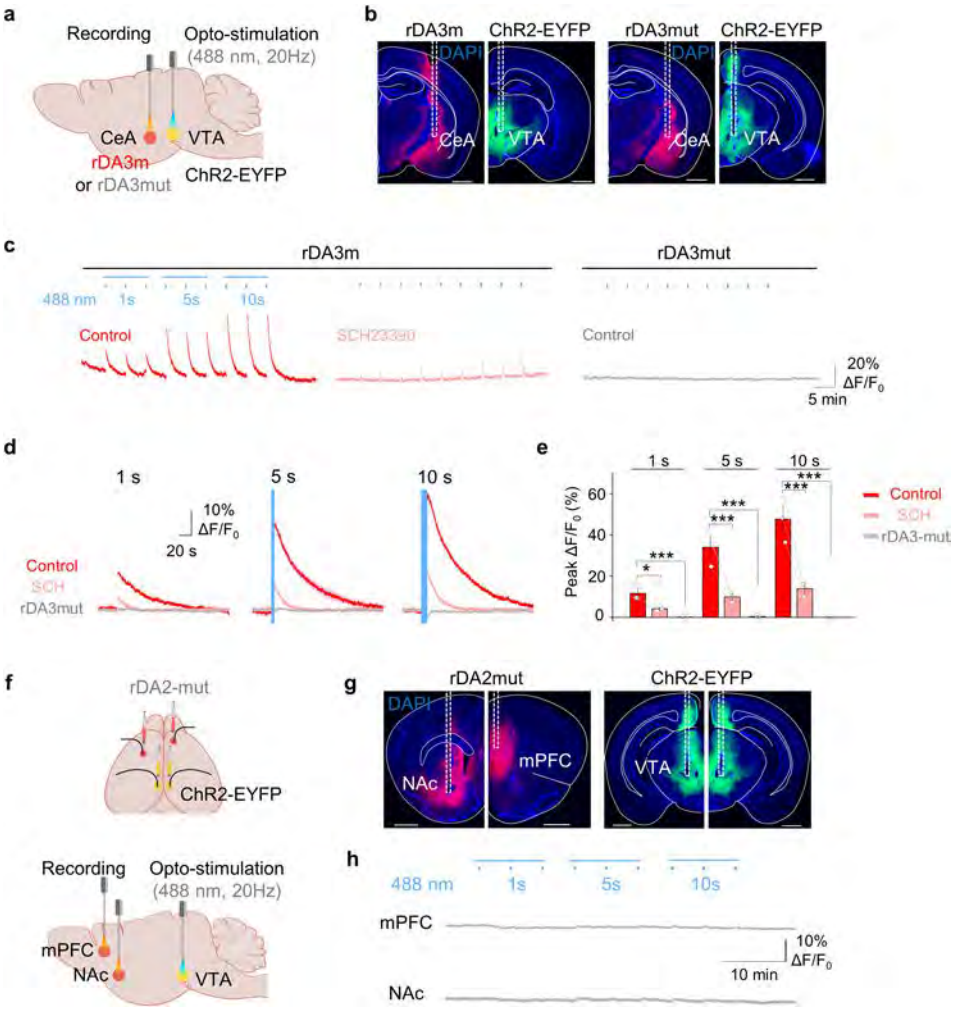

Extended Data Fig. 5 | rGRAB sensors report optogenetically-elicited DA release in multiple brain regions *in vivo*. **a**, Schematic illustration depicting the experimental design for panel **b**-**e**. **b**, Histological verification of indicated sensor expression in CeA and ChrimsonR expression in VTA. Dashed boxes indicate the location of optical tract. Scale bar, 1 mm. **c**, Representative traces of rDA3m or rDA3mut signals during optogenetic stimulations. rDA3m signals were measured before and after SCH-23390 (SCH) administration. **d**, Average traces of the change in sensor fluorescence to 1-, 5- or 10-s opto-stimulation from a mouse. Data are shown as mean ± SD. The blue shaded area indicates the application of opto-stimulation. **e**, Group summary of peak response of rDA3m or rDA3mut to indicated optogenetic stimulation. $n = 3$ mice for rDA3m and $n = 5$ for rDA3mut, mean±s.e.m. Two-tailed Student's t-test was performed. p = 0.0278, 0.0101, 0.0068 between control and SCH to 1-, 5-, 10-s opto-stimulation. p = 0.0003, 0.0001, 0.00004 between rDA3m and rDA3mut to 1-, 5-, 10-s opto-stimulation. **f**, Schematic illustration depicting the experimental design for panel **g**, **h**. **g**, Histological verification of rDA2mut expression in mPFC and NAc, and ChrimsonR expression in VTA. Dashed boxes indicate the location of optical tract. Scale bar, 1 mm. **h**, Representative traces of rDA2mut signals simultaneously recorded in the mPFC (top) and NAc (bottom) during optogenetic stimulations.

https://doi.org/10.1038/s41592-023-02100-w

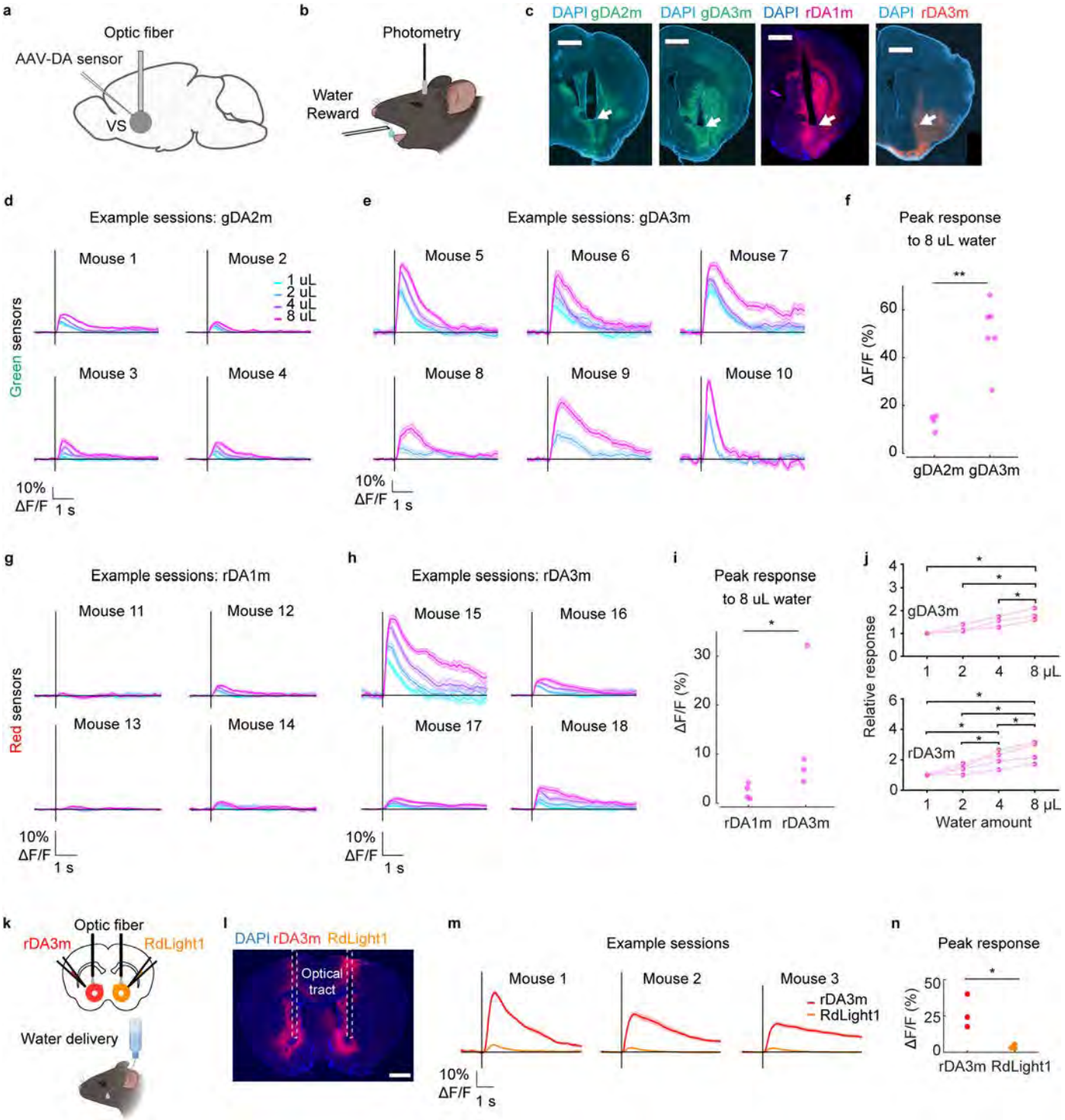

Extended Data Fig. 6 | *In vivo* comparison of the third-generation DA sensors versus previous variants in water-restricted mice receiving water rewards. **a**, Diagram of mouse surgical procedure. AAVs carrying $gGRAB_{DA2m}$, $gGRAB_{DA3m}$, $rGRAB_{DA1m}$, or $rGRAB_{DA3m}$ were injected unilaterally into NAc. An optic fiber was implanted above the injection site. **b**, Illustration of behavioral experiment. **c**, Histological verification of indicated sensor expression in NAc. White arrows indicate the location of fiber tips. Scale bar, 1 mm. **d**, Recording sessions from gDA2m mice, mean±s.e.m. Vertical black bars indicate water delivery. Colors indicate water volume. **e**, Recording sessions from gDA3m mice, mean±s.e.m. **f**, Peak response to 8 μL water for the sessions shown in **d** and **e**. n = 4 mice for gDA2m, n = 6 for gDA3m. p = 0.0095, Two-tailed Mann-Whitney U test. **g**, Recording sessions from rDA1m mice, mean±s.e.m. **h**, Recording sessions from rDA3m mice, mean±s.e.m. **i**, Peak response to 8 μL water for the sessions shown in **g** and **h**. n = 4 for rDA1m, n = 4 for rDA3m. p = 0.0286, Two-tailed Mann-Whitney U test. **j**, Group summary of sensor responses to each water amount. The response of each mouse was relative to that to 1 μL water reward. *n* = 3 mice for gDA3m, *n* = 4 mice for rDA3m. Two-tailed Student's t-test was performed between groups. For gDA3m, p = 0.032, 0.0185 and 0.0312 between 1, 2, 4 vs 8 μL, respectively; For rDA3m, p = 0.0217, 0.017 and 0.0179 between 1, 2, 4 vs 8 μL, and p = 0.032 and 0.0378 between 1, 2 vs 4 μL respectively. **k**, Schematic illustration depicting the mouse surgical procedure and the experimental design for panel **l**-**n**. **l**, Histological verification of rDA3m (left side) and RdLight1 (right side) in NAc. Dashed boxes indicate the location of optical tract. Scale bar, 1 mm. **m**, Recording sessions from 3 mice. Vertical black bars indicate water delivery. Colors indicate sensor version. **n**, Peak response of rDA3m and RdLight1 for the sessions shown in **m**. *n* = 3 mice for rDA3m and RdLight1. p = 0.0249, Two-tailed Student's t-test.

https://doi.org/10.1038/s41592-023-02100-w

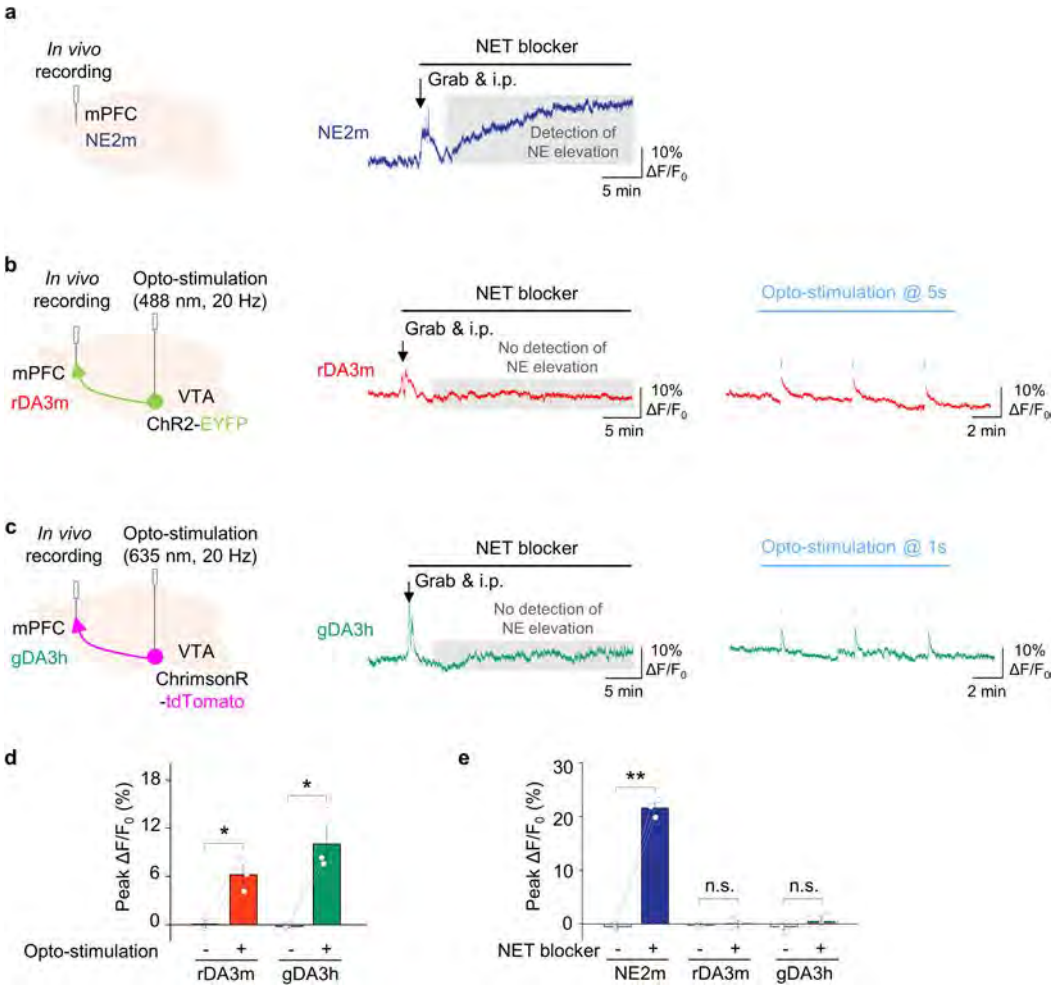

Extended Data Fig. 7 | GRAB$_{DA}$ sensors show minimal signal changes towards endogenous NE elevation. a, Schematic illustration (left) depicting the experimental design and representative fluorescence changes of NE2m towards systematic administration of NET blocker (3 mg/kg desipramine). **b**, Schematic illustration (left) depicting the experimental design and representative fluorescence changes of rDA3m towards systematic administration of NET blocker (middle) and upon optogenetic stimulations (right). **c**, Schematic illustration (left) depicting the experimental design and representative fluorescence changes (right) of gDA3h towards systematic administration of NET blocker (middle) and upon optogenetic stimulations (right). **d**, Group summary of $\Delta F/F_0$ for the indicated sensors upon opto-stimulation of VTA neurons. $n = 3$ mice for rDA3m and gDA3h, mean±s.e.m. Paired two-tailed Student's t-test was performed within group. *p = 0.0167 for rDA3m and *p = 0.0463 for gDA3h. **e**, Group summary of $\Delta F/F_0$ for the indicated sensors towards systematic administration of NET blocker. $n = 3$ mice for NE2m, rDA3m and gDA3h, respectively, mean±s.e.m. Paired two-tailed Student's t-test was performed within group. p = 0.6827, 0.2155 and 0.0012 for rDA3m, gDA3h and NE2m.

https://doi.org/10.1038/s41592-023-02100-w

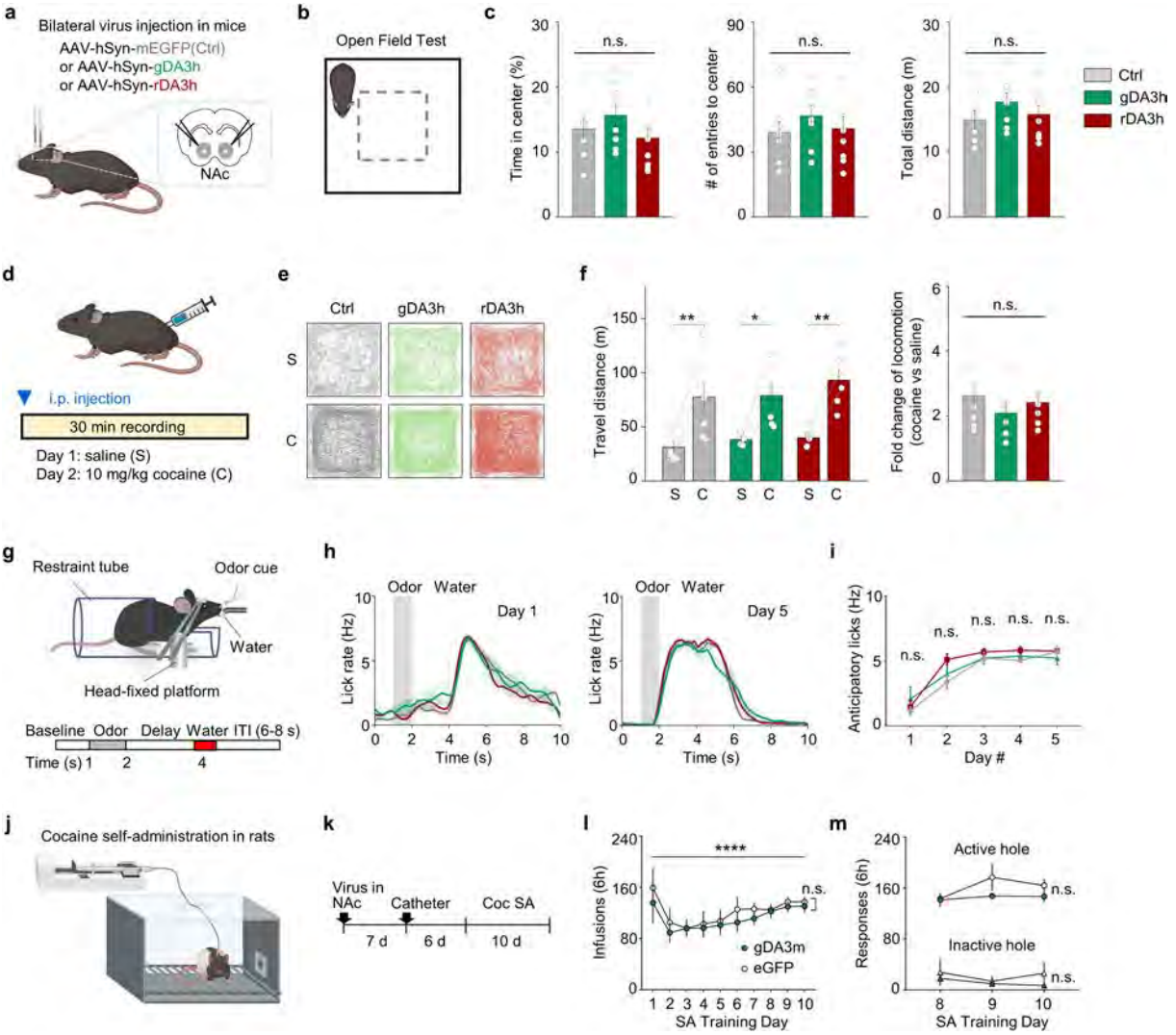

Extended Data Fig. 8 | GRAB$_{DA}$ expression in NAc has minimal effects on DA-related animal behaviors. a, Schematic representation of viral injections in the bilateral NAc. **b**. Schematic illustration showing the open field test (OFT). **c**, Quantification of behavioral parameters in the OFT. *n* = 8, 8 and 10 mice for the control, gDA3h and rDA3h group, respectively, mean±s.e.m. One-way ANOVA was performed. p = 0.3118, 0.5870 and 0.3736. **d**, Schematic illustration depicting the experimental designs for panel **e**-**f**. **e**, Representative track of control, gDA3h and rDA3h animals. **f**, Quantification of behavioral parameters during the experiments. *n* = 8, 6 and 6 mice for the control, gDA3h and rDA3h group, respectively, mean±s.e.m. Two-tailed Student's t tests were performed within groups: p = 0.0026, 0.0196 and 0.0039; One-way ANOVA was performed among groups: p = 0.6016. **g**, Schematic illustration showing the odor-reward associative learning task. **h**, Mean lick rate of Ctrl, gDA3h and rDA3h mice on day 1 and day 5 conditioning. *n* = 5 mice for each, mean±s.e.m. **i**, Quantification of anticipatory lick rate across five conditioning days. *n* = 5 mice for each, mean±s.e.m. Two-way ANOVA was performed among groups, p = 0.1076. **j**, Schematic diagram illustrating intravenous cocaine self-administration in rats. **k**, Timeline describing intravenous cocaine self-administration experiments. **l**, Cocaine infusions over 10 days of SA training did not differ between rats expressing gDA3m and eGFP virus bilaterally in the NAc core. *n* = 8 rats for each, mean±s.e.m. Two-way ANOVA mixed-effects model (Day x Virus): Day, F(9,126) = 4.50, p = 0.00004; Virus, F(1,14) = 0.35, p = 0.56; Day x Virus, F(9,126) = 0.21, p = 0.99. **m**, Nose-pokes in the active and inactive ports over the last 3 days of SA training did not differ between virus groups. Two-way ANOVA mixed-effects models (Day x Virus). *n* = 8 rats for each, mean±s.e.m. Active port: Day, F(2,28) = 3.21, p = 0.06; Virus, F(1,14) = 1.35, p = 0.27; Day x Virus, F(2,28) = 1.48, p = 0.24. Inactive port: Day, F(2, 28) = 1.97, p = 0.16; Virus, F(1,14) = 0.48, p = 0.50; Day x Virus, F(2,28) = 0.92, p = 0.41.

https://doi.org/10.1038/s41592-023-02100-w

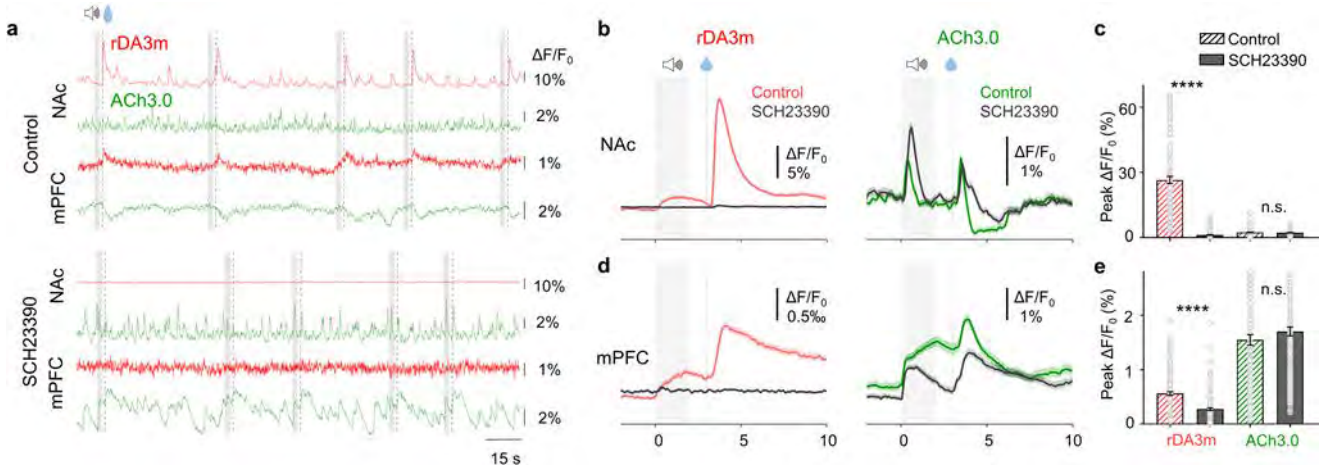

Extended Data Fig. 9 | The signals in the mouse NAc and mPFC during Pavlovian conditioning. a, Representative fluorescence signals recorded during consecutive water trials pre (top, control) and post SCH-23390 (bottom, SCH-23390) treatment. The audio and water delivery are indicated above. **b**, Averaged traces of rDA3m (left) and ACh3.0 (right) fluorescence measured in the NAc from a mouse under control condition or in the presence of SCH-23390 in one mouse, mean±s.e.m. The grey shaded area indicates the application of audio. The dashed line indicates the delivery of water. **c**, Group summary of the peak fluorescence change of rDA3m and ACh3.0 signals in the NAc under the indicated condition. $n = 155$ trials from 3 mice for each group, mean±s.e.m. Two-tailed Student's t-test was performed between control and SCH-23390 group. p = 0.2624 for ACh3.0. **d**, **e**. same as (**b**, **c**) with simultaneously recorded rDA3m and ACh3.0 signals in the mPFC. Two-tailed Student's t-test was performed between control and SCH-23390 group. p = 0.2274 for ACh3.0.

https://doi.org/10.1038/s41592-023-02100-w

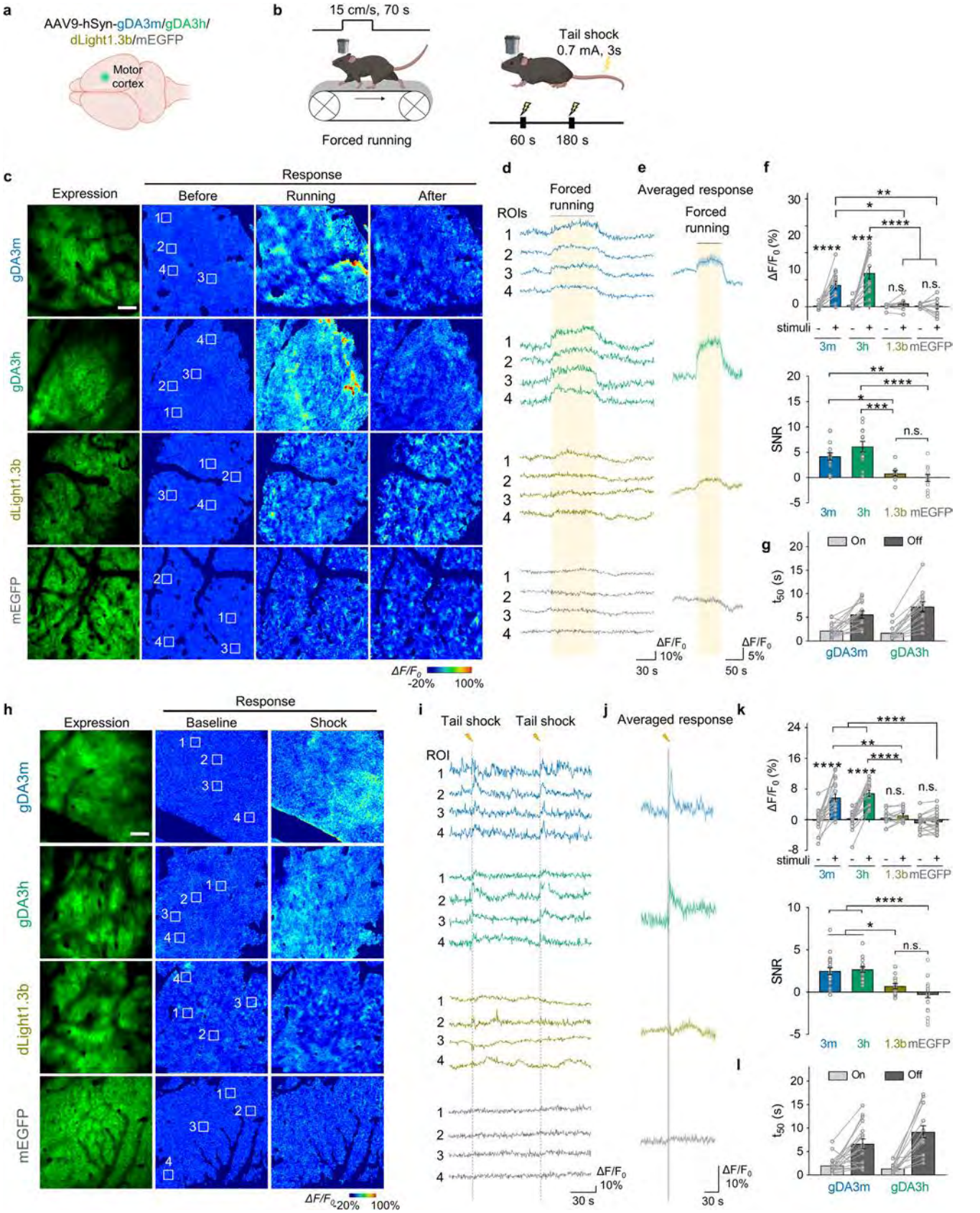

Extended Data Fig. 10 | See next page for caption.

https://doi.org/10.1038/s41592-023-02100-w

Extended Data Fig. 10 | *In vivo* two-photon imaging of cortical DA dynamics in mice. a, **b**, Schematic illustration depicting the experimental design for panel **c**-**j**. **c**–**e**, Representative expression and pseudocolored response images (**c**), representative traces measured at the indicated ROIs (**d**), and average traces per forced running (**e**) measured in the motor cortex expressing indicated sensors. Scale bar, 100 µm. **f**, Group summary of the peak response (top) and SNR (bottom) of indicated sensors measured during forced running. n = 14/4 (14 trials from 4 mice), 13/4, 9/3 and 12/4 for gDA3m, gDA3h, dLight1.3b and mEGFP, respectively, mean±s.e.m. Paired two-tailed Student's t-test was performed for response: $p = 6 \times 10^{-5}$, 0.0002, 0.0683, 0.6275 for gDA3m, gDA3h, dLight1.3b and mEGFP. One-way ANOVA, post hoc Tukey's test was performed across groups: response, $p = 9 \times 10^{-5}$, 4×10^{-6}, 0.0214, 0.0022, 0.1611 and 0.9577 between gDA3h and dLight1.3b, gDA3h and EGFP, gDA3m and dLight1.3b, gDA3m and mEGFP, gDA3m and gDA3h, and dLight1.3b and mEGFP, respectively; SNR, $p = 9 \times 10^{-6}$, 0.0004, 0.0016, 0.0337 and 0.8812 between gDA3h and mEGFP, gDA3h and dLight1.3b, gDA3m and mEGFP, gDA3m and dLight1.3b, and dLight1.3b and mEGFP, respectively. **g**, Summary of the rise and decay t_{50} values of indicated sensors to forced running. n = 14/4 for gDA3m, n = 13/4 for gDA3h, mean±s.e.m. **h**–**j**, Same as (**c**-**e**) except mice were subjected to tail shock. **k**, Group summary of the response (top) and SNR (bottom) of indicated sensors measured upon tail shock. n = 19/4 for gDA3m, 16/4 for gDA3h, 12/3 for dLight1.3b, 26/4 for mEGFP, mean±s.e.m. Paired two-tailed Student's t-test was performed for response: $p = 3 \times 10^{-5}$, 4×10^{-7}, 0.1774 and 0.2554 for gDA3m, gDA3h, dLight1.3b and mEGFP. One-way ANOVA, post hoc Tukey's test was performed across groups: response, $p = 8 \times 10^{-5}$, 1×10^{-8}, 0.0.0013, 4×10^{-8}, 0.7169 and 0.3714 between gDA3h and dLight1.3b, gDA3h and EGFP, gDA3m and dLight1.3b, gDA3m and mEGFP, gDA3m and gDA3h, and dLight1.3b and mEGFP, respectively; SNR, $p = 1 \times 10^{-7}$, 0.0104, 1×10^{-6}, 0.0186 and 0.2607 between gDA3h and mEGFP, gDA3h and dLight1.3b, gDA3m and mEGFP, gDA3m and dLight1.3b, and dLight1.3b and mEGFP, respectively. **l**, Summary of the rise and decay t_{50} values of indicated sensors to tail shock. mEGFP data replotted from Fig. 6f. n = 18/4 for gDA3m, n = 15/4 for gDA3h, mean±s.e.m.

nature portfolio

Corresponding author(s): Yulong Li

Last updated by author(s): Sep 26, 2023

Reporting Summary

Nature Portfolio wishes to improve the reproducibility of the work that we publish. This form provides structure for consistency and transparency in reporting. For further information on Nature Portfolio policies, see our Editorial Policies and the Editorial Policy Checklist.

Statistics

For all statistical analyses, confirm that the following items are present in the figure legend, table legend, main text, or Methods section.

n/a	Confirmed	
☐	☒	The exact sample size (*n*) for each experimental group/condition, given as a discrete number and unit of measurement
☐	☒	A statement on whether measurements were taken from distinct samples or whether the same sample was measured repeatedly
☐	☒	The statistical test(s) used AND whether they are one- or two-sided *Only common tests should be described solely by name; describe more complex techniques in the Methods section.*
☒	☐	A description of all covariates tested
☐	☒	A description of any assumptions or corrections, such as tests of normality and adjustment for multiple comparisons
☐	☒	A full description of the statistical parameters including central tendency (e.g. means) or other basic estimates (e.g. regression coefficient) AND variation (e.g. standard deviation) or associated estimates of uncertainty (e.g. confidence intervals)
☐	☒	For null hypothesis testing, the test statistic (e.g. *F*, *t*, *r*) with confidence intervals, effect sizes, degrees of freedom and *P* value noted *Give P values as exact values whenever suitable.*
☒	☐	For Bayesian analysis, information on the choice of priors and Markov chain Monte Carlo settings
☒	☐	For hierarchical and complex designs, identification of the appropriate level for tests and full reporting of outcomes
☒	☐	Estimates of effect sizes (e.g. Cohen's *d*, Pearson's *r*), indicating how they were calculated

Our web collection on statistics for biologists contains articles on many of the points above.

Software and code

Policy information about availability of computer code

Data collection	Below is the software used for data collection in this manuscript 1. The NIS-Element 4.51.00 software of Ti-E A1 confocal microscope (Nikon) 2. The FV10-ASW Ver.3.1a software of FV1000MPE 2-photon microscope (Olympus) 3. The Prairie View 5.5 software of Ultima Investigator 2-photon microscope (Bruker) 4. The Harmony 4.9 software of Opera Phenix high-content screening system (Perkin Elmer) 5. The Aperio VERSA software of Leica Aperio Versa (Leica) 6. The Multi Channel Fiber Photometry software of the fiber-photometry system (Thinkerbiotech, China) 7. The Inper signal V2.0.0 software of the fiber-photometry system (Inper, China) 8. The ScanImage 3.8.1 software 9. The Activity Monitor 7 software (Med Associates)
Data analysis	Below is the software used for data analysis in this manuscript 1. ImageJ version1.53c 2. Matlab R2020a and R2022a 3. OriginPro 2020b 4. GraphPad Prism 8.0.2 5. Adobe Illustrator CC 6. EZcalcium motion correction algorithm

For manuscripts utilizing custom algorithms or software that are central to the research but not yet described in published literature, software must be made available to editors and reviewers. We strongly encourage code deposition in a community repository (e.g. GitHub). See the Nature Portfolio guidelines for submitting code & software for further information.

Data

Policy information about availability of data

All manuscripts must include a data availability statement. This statement should provide the following information, where applicable:

- Accession codes, unique identifiers, or web links for publicly available datasets
- A description of any restrictions on data availability
- For clinical datasets or third party data, please ensure that the statement adheres to our policy

human (hORFeome database 8.1); The plasmids and sequences used to express the sensors in this study are available from Addgene (catalog nos. 208692 to 208708); The custom-written code has been uploaded in the github; source data are provided with the paper.

Human research participants

Policy information about studies involving human research participants and Sex and Gender in Research.

Reporting on sex and gender	N/A
Population characteristics	N/A
Recruitment	N/A
Ethics oversight	N/A

Note that full information on the approval of the study protocol must also be provided in the manuscript.

Field-specific reporting

Please select the one below that is the best fit for your research. If you are not sure, read the appropriate sections before making your selection.

☒ Life sciences ☐ Behavioural & social sciences ☐ Ecological, evolutionary & environmental sciences

For a reference copy of the document with all sections, see nature.com/documents/nr-reporting-summary-flat.pdf

Life sciences study design

All studies must disclose on these points even when the disclosure is negative.

Sample size	No statistical methods were used to predetermine sample size. Sample size are indicated for each experiment and were chosen based on similar studies (Sun, et al, Nat Methods, 2020 and Jing, et al, Nat Methods, 2020).
Data exclusions	No data was excluded from the analysis.
Replication	Each data in this manuscript is reliably reproducible. The replication number of each data is indicated in the legend of corresponding figures.
Randomization	Animals or cells were randomly assigned into experimental or control groups.
Blinding	The investigator were not blinded to group allocation during data collection and analysis. The experimental conditions were obvious to the researchers and the analyses were performed objectively and not subjective to human bias.

Reporting for specific materials, systems and methods

We require information from authors about some types of materials, experimental systems and methods used in many studies. Here, indicate whether each material, system or method listed is relevant to your study. If you are not sure if a list item applies to your research, read the appropriate section before selecting a response.

Materials & experimental systems

n/a	Involved in the study
☐	☒ Antibodies
☐	☒ Eukaryotic cell lines
☒	☐ Palaeontology and archaeology
☐	☒ Animals and other organisms
☒	☐ Clinical data
☒	☐ Dual use research of concern

Methods

n/a	Involved in the study
☒	☐ ChIP-seq
☒	☐ Flow cytometry
☒	☐ MRI-based neuroimaging

Antibodies

Antibodies used

Primary antibodies:
1. chicken anti-GFP (1:1000, Abcam, Cat # ab13970)
2. rabbit anti-RFP (1:500, Rockland Immunochemicals, Cat # 600-401-379)

Secondary antibodies:
1. Alexa Fluor® 488 goat anti-chicken IgY (H+L) (1:500, Abcam, Cat # ab150169)
2. iFluor® 555 goat anti-rabbit IgG (H+L) (1:500, AAT Bioquest, Cat # 16690)

Validation

All antibodies were validated by the manufacturer and published research articles.
Chicken anti-GFP antibody (Abcam) used in immunofluorescence has been verified in Al-Moyed H, et al, EMBO Mol Med, 2019 and Handara G, et al, eLife, 2015.
Rabbit anti-RFP antibody (Rockland Immunochemicals) used in immunofluorescence has been verified in Deng, et al, Cell, 2021 and Muller PA et al, Nature, 2020.

Eukaryotic cell lines

Policy information about cell lines and Sex and Gender in Research

Cell line source(s)

HEK293T (ATCC cat. no. 3216), HTLA cells (HEK293 cells stably expressing a tTA-dependent luciferase reporter and β-arrestin2-TEV fusion construct) were kindly provided by Dr. Richard Axel, Columbia University.

Authentication

The cell lines were authenticated based on the morphology under microscope and the analysis of the growth curve.

Mycoplasma contamination

No mycoplasma contamination.

Commonly misidentified lines
(See ICLAC register)

No commonly misidentified cell lines were used.

Animals and other research organisms

Policy information about studies involving animals; ARRIVE guidelines recommended for reporting animal research, and Sex and Gender in Research

Laboratory animals

For cultured cortical neurons, both male and female Sprague-Dawley rats (postnatal day 0, P0) were used; For ex vivo experiments, either adult (P42-P90) wild-type C57BL/6N (Beijing Vital River laboratory)
or TH-Cre (The Jackson Laboratory) mice of both sexes were used; For in vivo experiments, adult wild-type C57BL/6J (Beijing Vital River laboratory), adult wild-type C57BL/6N (Beijing Vital River laboratory), DAT-Cre (The Jackson Laboratory) and Long Evans Rats (> 10 weeks, Charles River) were used.

Wild animals

No wild animals were used in the study.

Reporting on sex

For the experiments (pavlovian conditioning task and two-photon in vivo imaging) that mice are head-fixed, we chose the female mice to reduce the likelihood of aggressive behaviors. As the male mice can be more aggressive than female, which could potentially interfere with experimental designs. Besides, female mice are preferred in the cognitive and learning studies, due to their differences in social behaviors and memory processes.

Field-collected samples

No field-collected samples were used in the study.

Ethics oversight

All procedures for animal surgery and experimentation were performed in accordance and approved by the laboratory animal care and use committees of Peking University, the Institutional Animal Care and Use Committee at Oregon Health and Science University, the National Institutes of Health Guide for the Care and Use of Laboratory Animals and Harvard Animal Care and Use Committee.

Note that full information on the approval of the study protocol must also be provided in the manuscript.